Cell Communication and Signaling

RESEARCH

Open Access

SIRT1 prevents noise-induced hearing loss by enhancing cochlear mitochondrial function

Yuelian Luo[1†], Haoyang Wu[1†], Xin Min[1†], Yi Chen[1], Wenting Deng[1], Minjun Chen[1], Chuxuan Yang[1] and Hao Xiong[2*]

Abstract

Exposure to traumatic noise triggers cochlear damage and consequently causes permanent sensorineural hearing loss. However, effective treatment strategies for noise-induced hearing loss (NIHL) are lacking. Sirtuin 1 (SIRT1) is a NAD^+-dependent deacetylase that plays a critical role in multiple physiological and pathological events. However, its role in NIHL pathogenesis remains elusive. This study revealed that SIRT1 expression in the cochlea progressively decreases in a mouse model of NIHL. Hair cell-specific knockout of SIRT1 exacerbates the noise-induced loss of outer and inner hair cell synaptic ribbons, retraction of cochlear nerve terminals, and oxidative stress, leading to more severe NIHL. Conversely, adeno-associated virus (AAV)-mediated SIRT1 overexpression effectively attenuated most noise-induced cochlear damage and alleviated NIHL. Transcriptomic analysis revealed that SIRT1 deficiency impairs glucose metabolism and inhibits antioxidant pathways in the cochlea following exposure to noise. Further investigation revealed that SIRT1 exerts an antioxidant effect, at least in part, through AMPK activation in cultured auditory HEI-OC1 cells exposed to oxidative stress. Collectively, these findings indicate that SIRT1 is essential for the maintenance of redox balance and mitochondrial function in the cochlea after traumatic noise exposure, thus providing a promising therapeutic target for NIHL treatment.

Keywords SIRT1 conditional knockout, Noise-induced hearing loss, Mitochondrial dysfunction, Sensory hair cells, AAV

†Yuelian Luo, Haoyang Wu and Xin Min contributed equally to this work.

*Correspondence:
Hao Xiong
xiongh@gdph.org.cn
Full list of author information is available at the end of the article

Graphical Abstract

Schematic illustration of SIRT1's protective role and mechanism in NIHL. Exposure to noise leads to downregulation of SIRT1 and phosphorylated AMPK (p-AMPK) levels, which subsequently triggers OHC loss, synaptopathy, and neurite retraction in the cochlea. This cascade results in mitochondrial dysfunction, which is characterized by reduced ATP production and increased ROS accumulation, with a concomitant decrease in antioxidant capacity. To counteract these adverse effects, AAV-mediated SIRT1 overexpression (AAV-SIRT1) has been explored as a therapeutic strategy to restore SIRT1 levels and protect against NIHL.

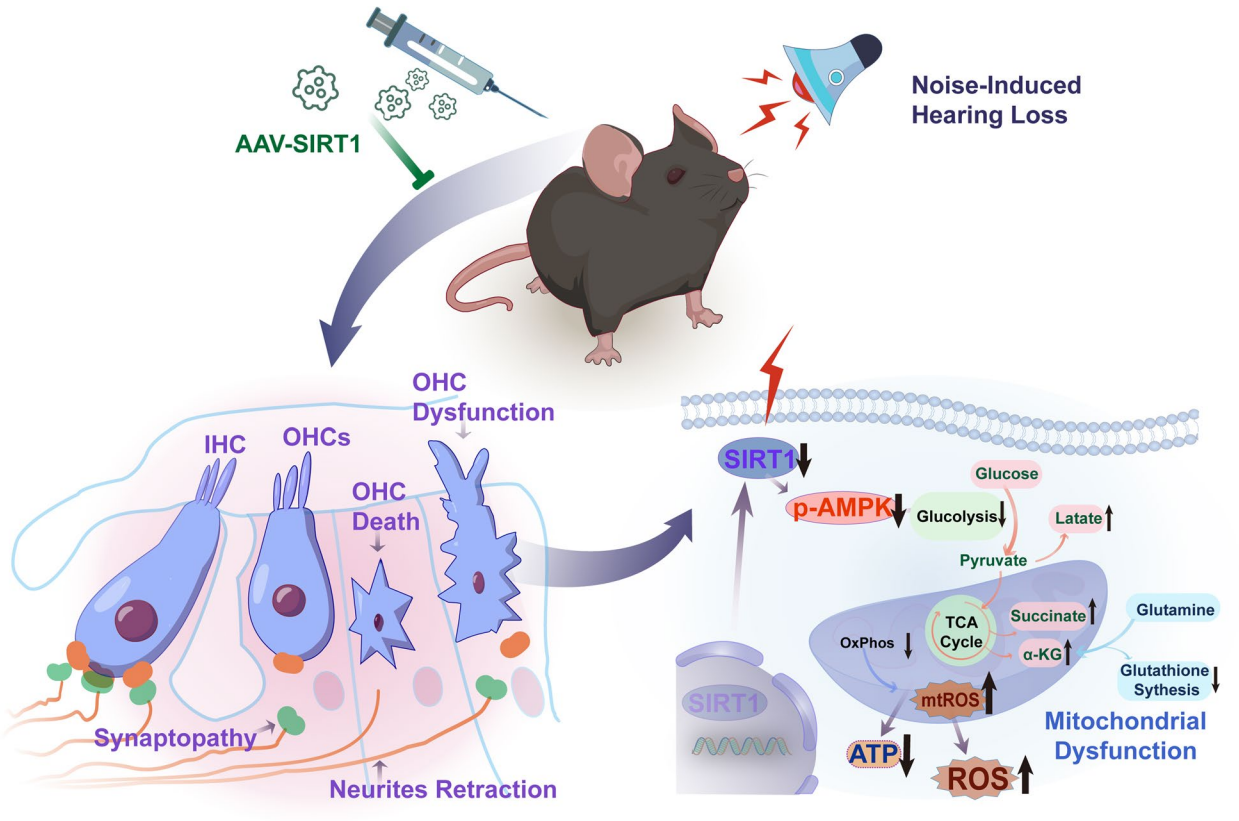

Introduction

Hearing loss is a widespread occupational and environmental health challenge, affecting over 430 million people worldwide, as reported by the World Health Organization [1]. Noise-induced hearing loss (NIHL) is the third most common cause of hearing impairment and is attributed to prolonged exposure to high-intensity noise levels [2]. Traumatic noise exposure leads to cochlear hair cell damage and disrupts connections with the auditory nerve, leading to hair cell dysfunction or death, synaptic loss, and nerve fiber degeneration [3–5]. Although the precise mechanisms underlying NIHL are not fully understood, reactive oxygen species (ROS) are well-documented as a general pathological mechanism of inner ear injuries [6, 7]. As mitochondria are responsible for generating over 90% of cellular ROS, mitochondrial dysfunction is a significant contributor to redox imbalance in the inner ear [8–10].

Sirtuin 1 (SIRT1) is a NAD^+-dependent deacetylase that plays a key role in regulating cellular metabolism, responses to stress, genomic stability, and mitochondrial function [11, 12]. By deacetylating critical target proteins such as PGC-1α and FOXO3a, SIRT1 promotes mitochondrial biogenesis, boosts antioxidant defenses, and enhances metabolic efficiency, which are all vital for maintaining mitochondrial homeostasis [13–16]. A deficiency in SIRT1 has been linked to numerous neurological and cardiovascular disorders [11, 17–19]. Our previous study showed that SIRT1 is broadly expressed in the mouse cochlea. Additionally, a significant decline

in SIRT1 expression in hair cells was noted shortly after noise exposure. Moreover, dietary supplementation with resveratrol mitigates noise-induced reduction in SIRT1 levels and prevents NIHL [20, 21]. Other studies have shown that enhancing SIRT1 activity using pharmacological agents can reduce different types of hearing loss, indicating that SIRT1 is a promising target for hearing protection [22, 23]. However, most of these nonspecific activators affect multiple target proteins in addition to SIRT1, and the specific downstream pathways through which SIRT1 protects the cochlea following noise exposure have not yet been fully elucidated.

This study aimed to clarify the role of SIRT1 in NIHL by generating hair cell-specific SIRT1-knockout and SIRT1-overexpressing mice. Furthermore, this study aimed to elucidate the protective mechanisms by which SIRT1 alleviates oxidative stress and enhances mitochondrial function in the cochlea following exposure to traumatic noise levels.

Methods

Animals

SIRT1 conditional knockout mice (genotype: *SIRT1* $^{flox/flox}$; *Gfi1* $^{cre/+}$) were generated by crossing heterozygous *SIRT1* ^{flox} mice with *Gfi1*^{cre} mice, which exhibited hair cell-specific Cre expression. Briefly, *SIRT1* $^{flox/flox}$ mice were initially bred with *Gfi1*^{cre} mice (both on a C57BL/6 J background and sourced from Cyagen Biosciences) to produce *SIRT1* $^{flox/+}$; *Gfi1* $^{cre/+}$ offsprings. These *SIRT1* $^{flox/+}$; *Gfi1* $^{cre/+}$ mice were then crossed with *SIRT1* $^{flox/flox}$ mice to obtain SIRT1 conditional knockout (*SIRT1* CKO) mice. Both male and female mice were included in this study, with *SIRT1* $^{flox/flox}$ littermates serving as controls. Five-week-old wild-type C57BL/6 J mice were acquired from the Experimental Animal Center of Sun Yat-sen University. All the procedures complied with the standards of animal care, welfare, and ethical considerations.

Genotyping

Genotyping was conducted by extracting DNA from the toe tissues of mice. The presence of the *SIRT1* ^{null} allele was detected using primers with the sequences 5′-GAG TTAGTCAGATGTAGGCCACC-3′ and 5′-GAGGCT CACAAACATCATCACTC-3′. The PCR protocol began with an initial denaturation step at 94 °C for 3 min, followed by 35 cycles including a 1-min denaturation at 94 °C, 1-min annealing at 58 °C, and 1-min extension at 72 °C. This was concluded with a final 10-min extension at 72 °C. *Gfi* ^{cre} was synthesized by the following primers: 5′-GCCCAAATGTTGCTGGATAGT-3′, 5′-GGG ATAACGGACCAGTTG-3′, and 5′-CCGAGGGGC GTTAGGATA-3′ and the conditions included were as follows: The first stage of the polymerization technique involves 3 min of boiling at 94℃. Then, there are 35 cycles consisting of 94℃-30-s denaturation, 58℃-45-s annealing, and 72℃-45-s extension, and finally, the final extension of 72℃ lasted for 10 min. The resulting PCR products were run on a 2% agarose gel and the genotypes of the mice were determined based on the viewed band sizes. The 340 bp band shows the insertion of the *SIRT1* ^{flox} allele, the 233 bp band is direct evidence of wild-type SIRT1, the 609 bp band is Gfi1, and the 672 bp band is Cre.

Delivery of an adeno-associated virus (AAV) vector

The AAV2/anc80L65 vector, carrying either SIRT1 or an empty vector with a CMV promoter and enhanced green fluorescent protein (CMV-SIRT1-P2A-eGFP-WPRE or CMV-eGFP-WPRE), was produced by BrainVTA (Wuhan, China) at a titer of 5×10^{12} GC/mL. The vector plasmid and experimental process are shown in Fig. 5A. C57BL/6 J pups (P2-3) were briefly placed on ice until they lost consciousness and then moved to an ice pad for surgery. The duration of the surgery was 5-10 min. The surgery was conducted on the left ear of each animal. Post the delivery of anesthesia, injections were performed by means of the posterior semicircular canals (PSC) using a glass micropipette (25 μm) controlled by a micromanipulator MICRO4 (World Precision Instruments, Inc.), and the quantity of AAV injected was monitored to be 1 μL per cochlea in 1 min. After injection, the skin incision was closed using a veterinary tissue adhesive (Millpledge Ltd., UK). The pups were then placed on a heating pad at 37℃ for 10 min and then were returned to their mothers to continue nursing until the weaning period is reached.

Noise exposure

Five-week-old mice were exposed to octave-band noise with a frequency range of 8–16 kHz and sound pressure level (SPL) of 108 dB for 2 h to induce a permanent threshold shift. Awake mice were individually placed in rectangular wire mesh cages measuring 9 cm×5 cm×5 cm. Noise exposure was performed in a chamber equipped with a speaker (#HG220-9, RADIN, Germany) powered by a Yamaha amplifier (#P9500S, Japan), a TDT RX6 multifunction processor, and a Tucker Davis Technologies attenuator (US). The sound intensity of the exposure was calibrated and measured using a portable sound level meter to ensure a consistent sound field, with measurements taken before and after exposure to verify stability. The control mice, which were kept under silence without speakers, were placed in the same chamber for 2 h.

Auditory brainstem response (ABR)

The mice were anesthetized with 1% amobarbital (50 mg/kg) and maintained under warm conditions. The active electrode was positioned on the forehead, the reference electrode was placed beneath the left ear pinna, and the ground electrode was positioned under the right ear. ABR thresholds at frequencies of 8, 16, and 32 kHz were measured in the left ear of each subject using the BioSig32 software associated with the TDT BioSig III system. The sound levels at each frequency were progressively lowered from 90 to 10 dB, with each subsequent stimulus reduced by 10 dB SPL relative to the previous level, and an average of 1024 responses was computed for analysis. The ABR threshold is defined as the lowest level at which a discernible response is produced. Wave I amplitude was calculated by measuring the voltage difference between the peak and trough of the initial wave, whereas latency was determined by measuring the time interval from the stimulus onset to the peak of the first wave.

Preparation of cochlear tissues

Mice were euthanized by cervical dislocation after being anesthetized. The temporal bones were rapidly dissected and transferred to ice-cold phosphate-buffered saline (PBS). The cochleae were carefully isolated under a stereomicroscope and the stapes bone was removed using fine forceps. A small hole (~0.5-mm diameter) was punctured at the apex of the cochlear capsule to facilitate perfusion. For fixation, 4% paraformaldehyde (#BL539A, Biosharp, China) was gently perfused through both round and oval windows using a 1-mL syringe with a 30-gauge needle until the perilymph was completely replaced. Cochleae were immersed in fresh 4% PFA and fixed overnight at 4 °C. Decalcification was performed using 10% EDTA (#E769616, Macklin, China; pH 7.4) at 4 °C with gentle agitation. The EDTA solution was replaced every 24 h, and the decalcification duration was adjusted to 5-7 days, based on bone softening (confirmed by needle penetration testing). After decalcification, tissues were rinsed three times in PBS (1 h each) to neutralize residual EDTA and stored in PBS at 4 °C for further processing.

Immunohistochemistry of cochlear tissues

Immunohistochemistry of the cochlear tissues was performed according to previously reported procedures [24, 25]. The cochlear samples were permeabilized in a fresh solution of 3% Triton X-100 for 30 min at room temperature. After three washes with PBS (10 min each), the tissues were blocked with 10% normal goat serum for 30 min at room temperature.

Outer hair cells (OHCs) and inner hair cells (IHCs) were labeled with myosin VIIa or phalloidin and subsequently co-stained with additional markers depending on the experimental objectives. These include markers of oxidative stress (3-nitrotyrosine (3NT) and 4-hydroxynonenal (4HNE)), neurofilaments (NF), SIRT1, and phosphorylated AMP-activated protein kinase alpha 1 (p-AMPK). Briefly, specimens were incubated at 4 °C for 48 h with primary antibodies at a 1:200 dilution: rabbit polyclonal anti-Myosin VIIa (#25-6790, Proteus Biosciences, US), Phalloidin (#CA1640 and #CA1670, Solarbio, China), mouse monoclonal anti-SIRT1 (#Ab110304, Abcam, UK), mouse monoclonal anti-3-NT (#N5538, Sigma-Aldrich, US), rabbit polyclonal anti-4-HNE (#46,545, Abcam, UK), mouse monoclonal anti-NF (#GB12144, Servicebo, China), and rabbit anti-Phospho-AMPKα1 antibody (#AP0871, Abclonal, China). The tissues were then treated with Alexa-Fluor-594 or Alexa-Fluor-488-conjugated secondary antibodies at a 1:200 dilution for 2 h at room temperature in the dark.

For the immunolabeling of IHC synapses, the colocalization of synaptic ribbons was analyzed by labeling CtBP2 (C-terminal binding protein 2) as a presynaptic marker and GluA2 (glutamate ionotropic receptor AMPA type subunit 2) as a postsynaptic marker. Briefly, specimens were incubated overnight in the dark at 37 °C with primary antibodies: mouse anti-CtBP2 IgG1 (#612,044, BD Biosciences, US) at a 1:200 dilution and mouse anti-GluA2 IgG2a (#MAB397, Millipore, US) also at 1:200. After three wash cycles, the tissues were incubated for 1 h at 37 °C in the dark with secondary antibodies conjugated to Alexa-Fluor-594 or Alexa-Fluor-488, both diluted to 1:200. After an additional three washes, the samples were placed in a 4 °C dark environment overnight with anti-Myosin VIIa. Finally, the tissues were treated overnight at 4 °C with Alexa Fluor 350-conjugated secondary antibody at a 1:200 dilution in darkness. Immunolabeled images were acquired using an Olympus FV3000 confocal microscope at 80×magnification, maintaining consistent Z-stack settings.

Quantification of OHCs, synaptic ribbons, and auditory nerve fibers

The number of OHCs was determined according to the established protocols [26]. Cochlear specimens were stained with Myosin VIIa, and the OHCs were tallied along the entire cochlear epithelium. Each slice of 0.5-mm distance of the epithelium was used for a cytocochleagram to detect the displacement of hair cells. IHC synaptic ribbons marked with CtBP2 and GluA2 in the cochlear preparations were enumerated as previously reported, and the number of CtBP2 puncta was counted [6]. Converted Z-stack images were collected at 2-μm intervals, and synaptic ribbon numbers were processed using the ImageJ (National Institutes of Health,

Bethesda, MD, U.S.) software version 1.46r. The count of type II auditory nerve fibers (ANFs) was performed at the apical, middle, and basal regions of the cochlea, averaging over a 100-μm span and using IHCs as reference points. Moreover, the fluorescence of auditory nerve fibers (including type I and type II) was imaged using a 63× oil-immersion objective with Z-stacks acquired at 2-μm intervals, and maximum intensity projection was applied to generate 2D images using ImageJ. To account for background variability, raw fluorescence values were normalized by subtracting the mean intensity of the adjacent non-neural regions within the same tissue section. The 100 μm-wide region of interest, spanning from the IHC base to the habenula perforata, was consistently defined across specimens. Mean intensity values (arbitrary units, a.u.) were quantified using the "Measure" tool in ImageJ with pixel saturation thresholds fixed at 0-4095 a.u.

Western blot analysis

Cochlear samples were harvested from the euthanized mice and snap-frozen in liquid nitrogen. The House Ear Institute-Organ of Corti 1 (HEI-OC1) cells were collected on ice using a cell scraper after washed with PBS. Protein extraction was conducted at 4 °C using pre-chilled RIPA buffer (#20-188, Merck Millipore, Germany) supplemented with protease and phosphatase inhibitors (#P997469, Macklin, China). For both HEI-OC1 cells and cochlear tissues, homogenized samples were centrifuged at 14,000 × g for 10 min to remove cellular debris and obtain soluble protein lysates. To separate protein homogenates (20 μg), SDS-polyacrylamide gel electrophoresis was used. The separated proteins were transferred to a 0.22 μm polyvinylidene fluoride transfer membrane which was subsequently blocked in Tris-buffered saline with Tween-20 (TBST) containing 5% skimmed milk (#FD6006, FDBIO, China) for 2 h at room temperature. Thereafter, the membranes were incubated for a total of 16 h at 4℃ with 1:1000 rabbit anti-SIRT1 (#9475, Cell Signaling Technology, US, 1:1000), mouse anti-AMPK (#sc-74461, Santa Cruz, US, 1:1000), rabbit anti-Phospho-AMPKα1 (#AP0871, Abclonal, China, 1:1000) or rabbit anti-β-actin (#AF5003, Beyotime, China, 1:1000) antibodies. The membranes were then flushed with TBST, injected with HRP-conjugated goat anti-rabbit (#A0208, Beyotime, China, 1:1000) or anti-mouse (#A0216, Beyotime, China, 1:1000) antibodies, and finally left at room temperature for 1 h. Protein bands were detected using chemiluminescence and visualized on film. The greyscales of the bands were measured using the ImageJ software for further analysis.

RNA extraction and quantitative real-time PCR (qRT-PCR)

RNA was extracted from the cochlea using an RNA Express purification kit (#RN001, Yeasen, China) according to the manufacturer's instructions. The RNA concentration was determined using a NanoDrop instrument (Thermo Fisher Scientific). cDNA was synthesized from the total RNA (500 ng) using an RNA Reverse Transcription Kit (#11,144; Yeasen, China). qRT-PCR was performed in three tubes using qPCR SYBR Green Master Mix (#11198ES08; Yeasen, China) in a Roche LightCycler Detection System (Roche LightCycler 480 II). The primer sequences are listed in Supplementary Table 1. β-actin served as a reference gene.

SIRT1 activity assay

Two cochleae from the same mouse were placed in one vessel in a tissue homogenizer. Total cochlear protein was extracted as a protein lysate using a protein extraction reagent. Approximately 200-μL protein lysates were incubated with 3-μg anti-SIRT1 antibody (#sc-74465, Santa Cruz, US). Protein A agarose beads (20 μL of 50% bead slurry) were introduced into protein lysate and the whole system was gently rocked for 3 h at 4℃. After immunoprecipitation, NAD^+-dependent deacetylase activity was measured using the SIRT1 Assay Kit (#ab156065, Abcam, US) according to the manufacturer's instructions. The fluorescence intensity was continuously recorded for 45 min at 2-min intervals using a microplate reader (BioTek, US), with excitation at 350 nm and emission at 460 nm.

Cell culture, lentiviral infection, and drug treatment

The HEI-OC1 cell line was acquired from Cyagen Biosciences (Guangzhou, China) and was grown in high-glucose Dulbecco's modified Eagle's medium (DMEM; Gibco BRL, US) supplemented with 10% fetal bovine serum (FBS; Biological Industries, Israel). The chamber was preset to 10% CO_2 at 33℃ during the culture phase. In vitro SIRT1-specific gene overexpression was achieved using a lentivirus carrying the virus. SIRT1-overexpressed virus (#GXDL0390480) and GFP-expressing empty vector virus were purchased from GeneChem Co., Ltd. (China). HEI-OC1 cells were grown in 6-well plates up to 60% confluency and then infected with lentivirus particles in the presence of 5 μg/mL polybrene at a multiplicity of infection of 30. The cells were cultured for at least 3 days before further experiments were performed. SIRT1 overexpression was evaluated using qRT-PCR and western blotting. Selleck Compound C (CC) (#S7306, US) was used at 10 μM to inhibit AMPK in vitro, based on a previous study [27].

RNA sequencing

Cochlear samples were collected 4 h after noise exposure, comprising five samples from *SIRT1* $^{flox/flox}$ animals and six from *SIRT1* CKO animals. RNA extraction, purification, and concentration analyses were performed by transcriptome sequencing. Sequencing was performed on an Illumina NovaSeq 6000 platform (150 × 2 bp) by Shanghai BIOZERON Co., Ltd. The raw paired-end reads were trimmed and quality-controlled using Trimmomatic with the specified parameters. Clean reads were individually aligned to the reference genome in the orientation mode using HISAT2. Differential expression analysis between two groups was performed using the EBSeq package in R. A gene was regarded as differentially expressed if there was a fold change of > 0.75 and a *p*-value of < 0.05.

Glucose metabolomics analysis

Cochlear samples from the noise-exposed mice were divided into two groups, each containing four samples. Each sample was prepared from 10 cochleae (yielding over 100 mg in total) and homogenized at 6.0 m/s for 60 s using a FastPrep-24 homogenizer (MP Biomedicals, USA) in 24 × 2 mL tubes. The homogenized samples were sonicated on ice twice, with each sonication cycle lasting 30 min, and subsequently centrifuged at 14,000 × g at 4 °C for 5 min to remove cellular debris. The resulting supernatants were analyzed using an Agilent 1290 Infinity LC ultra-high-performance liquid chromatography (UHPLC) system coupled to a 5500 QTRAP mass spectrometer (SCIEX) operating in the negative ion mode. Chromatographic peak areas and retention times were analyzed using Multiquant 3.0.2 software, and metabolites were identified by matching retention times with reference standards.

Cell viability assay

Cell Counting Kit-8 (CCK-8; #K1018, Apex BIO, US) was used to detect the viability of HEI-OC1 cells. The density of the 96-well plate was 5000 cells/well, and the cells were incubated overnight under growth conditions. The cells were then incubated with different concentrations of hydrogen peroxide solution (H_2O_2; #7722-84-1, Sigma-Aldrich, US) for 30 min. After treatment, 10% CCK-8 solution was added to each plate; then the plates were incubated at 33℃ in 10% CO_2 for 2 h. Finally, we measured the optical density (OD) values using a microplate reader (Bio Tek, US) at 450 nm. The average OD in the control cells was considered to indicate 100% viability.

MitoSOX detection

Mitochondrial superoxide levels were measured using the MitoSOX Red Mitochondrial Superoxide Indicator (#40778ES50, Yeasen Biotechnology Co., Ltd., China) according to the manufacturer's protocol. Cells of HEI-OC1 were subjected to 5 mM of hydrogen peroxide for 30 min and later treated with 5 μM MitoSOX Red dye for 10 min. After staining, the cells were washed with Hank's balanced salt solution and counterstained with Hoechst 33,342 for 10 min. Finally, the stained cells were observed and photographed using a confocal microscope.

Adenosine triphosphate measurements

The levels of adenosine triphosphate (ATP) in the cochlear tissue and cells were determined using an ATP assay kit (#S0026, Beyotime, China). The samples of cochlear tissue were collected after noise exposure, and 100 μL of ATP lysis buffer was added. The tissue was completely ground in a grinder, centrifuged at 12,000 × g for 10 min at 4℃, and the supernatant collected. In relation to the cells, after H_2O_2 treatment, the culture medium was drained off, cells were washed with PBS, and 100 μL of ATP lysis buffer was added. The cells were then shaken in an incubator for 15 min. The lysate was collected, centrifuged at 12,000 × g for 5 min at 4℃, and the supernatant collected. ATP detection buffer was added and ATP levels were measured using a microplate reader (BioTek, US). The final ATP levels were normalized to protein content, rendering them equal.

Statistics and reproducibility

GraphPad Prism 8.0 was used to perform statistical analyses and create graphical visualizations with data shown as the mean values ± SD, derived from a minimum of three independent experiments. Two-way analysis of variance (ANOVA) was used for the analysis of ABR threshold data, OHC loss along the cochlear spiral, synapse loss, and nerve fiber loss. One-way ANOVA along with multiple comparison tests was utilized for multi-group comparisons, and two-tailed Student's t-tests were used for single-pair comparisons. Statistical significance was defined as a *p*-value < 0.05.

Study approval

All procedures were conducted in accordance with the ethical guidelines and approved by the Animal Ethics and Welfare Committee of Sun Yat-sen Memorial Hospital, Sun Yat-sen University (Approval No.: AP20220236).

Results

SIRT1 expression and activity is downregulated following noise exposure

To systematically explore the impact of acoustic trauma on SIRT1 in mouse cochlear hair cells, 5-week-old C57BL/6 J mice were subjected to noise at 108 dB SPL for 2 h, based on a previously demonstrated protocol to induce NIHL in mouse models [28]. The mammalian cochlea houses two functionally distinct sensory cell populations: OHCs act as biological amplifiers through somatic electromotility to enhance auditory sensitivity and frequency selectivity, while IHCs serve as primary mechanoelectrical transducers responsible for synaptic transmission to afferent neurons [29–31]. Given the distinct frequency ranges of mouse hearing, different cochlear regions (apex, middle, and basal turns) were examined (Fig. 1A). ABR measurements were conducted before and at 4 h, 24 h, and 7 days after noise exposure. Moreover, a parallel cohort was used to evaluate auditory function and observe the dynamic changes in SIRT1 expression and activity at these time points (Fig. 1B).

A significant elevation in ABR thresholds at 8, 16, and 32 kHz was observed at 4 h post-exposure, that partially recovered by 24 h, stabilizing at 70-80 dB by day 7 (Supplemental Fig. 1A). OHC loss along the cochlear spiral was quantified, revealing predominantly middle and basal localization with no detectable loss of IHCs. OHC loss was minimal at 4 and 24 h post-exposure but progressively increased by day 7, with average losses reaching 6% at 5 mm from the apex (Supplemental Fig. 1, B-C).

Further investigation using immunofluorescence and western blotting demonstrated that SIRT1 levels were near baseline at 4 h post-exposure, declined markedly by 24 h, and persisted at reduced levels until day 7 (Fig. 1, C-F). Additionally, SIRT1 activity, as evaluated using a SIRT1 activity assay, mirrored this dynamic decline (Fig. 1G). These results corroborate previous findings [32], underscoring the pivotal role of SIRT1 in the cochlear response to noise-induced auditory dysfunction.

SIRT1 deficiency heightens susceptibility to NIHL and hair cell loss

To investigate the role of SIRT1 in NIHL, we crossed cochlear hair cell-specific Gfi1-Cre (*Gfi1*$^{cre/+}$) mice to obtain SIRT1 hair cell-specific knockout mice (*SIRT1* CKO) (Supplemental Fig. 2, A-B). Deletion of SIRT1 was confirmed by PCR analysis of DNA from mouse toes (Supplemental Fig. 2C). In addition, *Gfi1*$^{cre/+}$ mice were crossed with Rosa26-tdTomato reporter line mice to verify Cre activity; robust tdTomato fluorescence in hair cells indicated successful recombination (Supplemental Fig. 2, D-E). Given that previous studies have reported progressive hearing loss in *Gfi1*$^{cre/+}$ mice [33], *Gfi1*$^{+/+}$; *SIRT1*$^{flox/flox}$ (denoted *SIRT1*$^{flox/flox}$ mice hereafter) were used as control mice. Immunofluorescence analysis confirmed the absence of SIRT1 expression in IHCs and OHCs of CKO mice (Supplemental Fig. 2F), whereas its expression in the cochlear lateral wall and spiral ganglion remained unaffected (Supplemental Fig. 2G). Western blotting further demonstrated an 78% reduction in SIRT1 protein levels in CKO mice relative to the controls (Supplemental Fig. 2, H-I). ABR measurements indicated that hearing function was normal in both *SIRT1*$^{flox/flox}$ and *SIRT1* CKO mice in the absence of noise (Supplemental Fig. 3A). Moreover, hematoxylin and eosin staining showed that the cochlear morphology was normal, and no significant difference was observed in body weight between *SIRT1*$^{flox/flox}$ and *SIRT1* CKO mice (Supplemental Fig. 3, B-D). Collectively, these findings confirmed the successful generation of a hair cell-specific SIRT1-knockout model, which is suitable for studying the functional role of SIRT1 in the auditory system.

Next, we evaluated the role of SIRT1 in protection against NIHL by exposing both *SIRT1* CKO and *SIRT1*$^{flox/flox}$ mice to noise at 108 dB SPL for 2 h and assessing hearing thresholds after 14 days (Fig. 2A). Noise exposure elevated ABR thresholds in both groups, while *SIRT1* CKO mice exhibited significantly greater threshold shifts, with a 20-dB increase across frequencies (8, 16, and 32 kHz) compared with controls (Fig. 2, B-C). We also measured the amplitude and latency of the ABR wave I, which reflects the functionality of the IHC ribbon synapses and spiral ganglion neurons. The amplitude of wave I was markedly reduced, and the latency was prolonged in *SIRT1* CKO mice, further highlighting the exacerbated auditory dysfunction in these mice (Fig. 2, D-F). Additionally, OHC loss was more pronounced in *SIRT1* CKO mice, with a 4% increase observed in the 5-mm region of the cochlear spiral from the apex compared to controls (Fig. 2, G-H). These findings demonstrate that absence of SIRT1 renders hair cells more vulnerable to noise-induced damage, leading to heightened hearing loss and increased cellular degeneration.

SIRT1 deficiency aggravates oxidative stress in hair cells following noise exposure

To elucidate the effect of SIRT1 on oxidative stress in cochlear hair cells, we measured 3NT, a marker of protein nitration, and 4HNE, a marker of lipid peroxidation and indicator of oxidative damage. Both *SIRT1*$^{flox/flox}$ and *SIRT1* CKO mice were used in the experiment and divided into four groups according to whether they were exposed to noise (i.e., *SIRT1*$^{flox/flox}$, *SIRT1* CKO, *SIRT1*$^{flox/flox}$ + noise, *SIRT1* CKO + noise). Immunofluorescence staining of the basal turn of the cochlea revealed that the

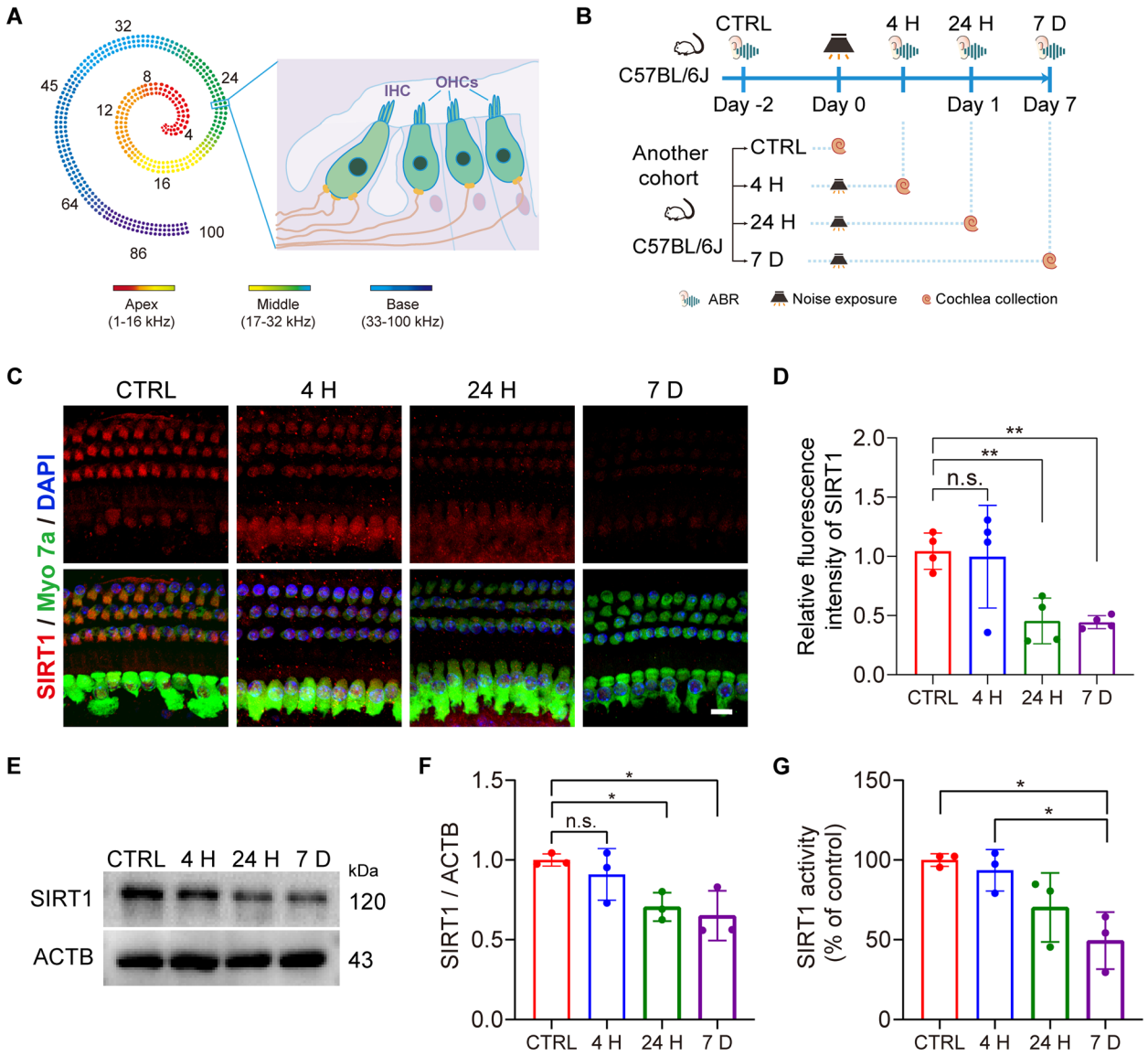

Fig. 1 Expression and activity of SIRT1 decreased following noise exposure. **A** The left panel shows a schematic diagram of mouse hearing frequencies, illustrating that hair cells from the apical to the basal turn correspond to the perception of low-to-high-frequency sounds. The right panel presents an enlarged diagram of an inner hair cell (IHC) and three outer hair cells (OHCs) within the organ of Corti. **B** Experimental design for noise exposure. Five-week-old C57BL/6 J mice were used. Auditory brainstem response (ABR) thresholds were measured pre-exposure and at 4 h, 24 h, and 7 day post-exposure. A separate cohort of mice was used for cochlea collection. **C**, **D** Representative images and quantifications showing reduced SIRT1-associated immunoreactivity (red) in IHCs and OHCs after noise exposure ($n = 4$ per group, with one cochlea analyzed per animal, one-way ANOVA with Tamhane's T2 post hoc testing). Myosin as a marker for cochlear hair cells (Myo 7a: myosin 7a). Cell nuclei were stained with DAPI (blue). Images were taken from the basal turn. Scale bar = 10 μm. **E**, **F** Western blots and densitometric analysis of SIRT1 in whole cochlear tissue homogenates. ACTB served as the loading control ($n = 3$ for each group, one-way ANOVA with Tukey's post hoc testing). **G** SIRT1 activity decreased after noise exposure ($n = 3$ for each group, one-way ANOVA with Tukey's post hoc testing). Data are presented as means ± SD. ns: not significant, * $p < 0.05$

fluorescence intensities of 3NT and 4HNE were low in both *SIRT1* $^{flox/flox}$ and *SIRT1* CKO mice under baseline conditions. However, after noise exposure, the fluorescence intensities of both markers increased significantly, with a greater increase observed in *SIRT1* CKO + noise mice than in *SIRT1* $^{flox/flox}$ + noise mice. This difference was statistically significant (Fig. 3, A-D), indicating that SIRT1 played a crucial role in mitigating noise-induced oxidative damage.

SIRT1 deficiency exacerbates synaptopathology and neurite retraction following noise exposure

Noise-induced loss of synaptic connections between IHCs and ANFs, as well as the retraction of cochlear nerve

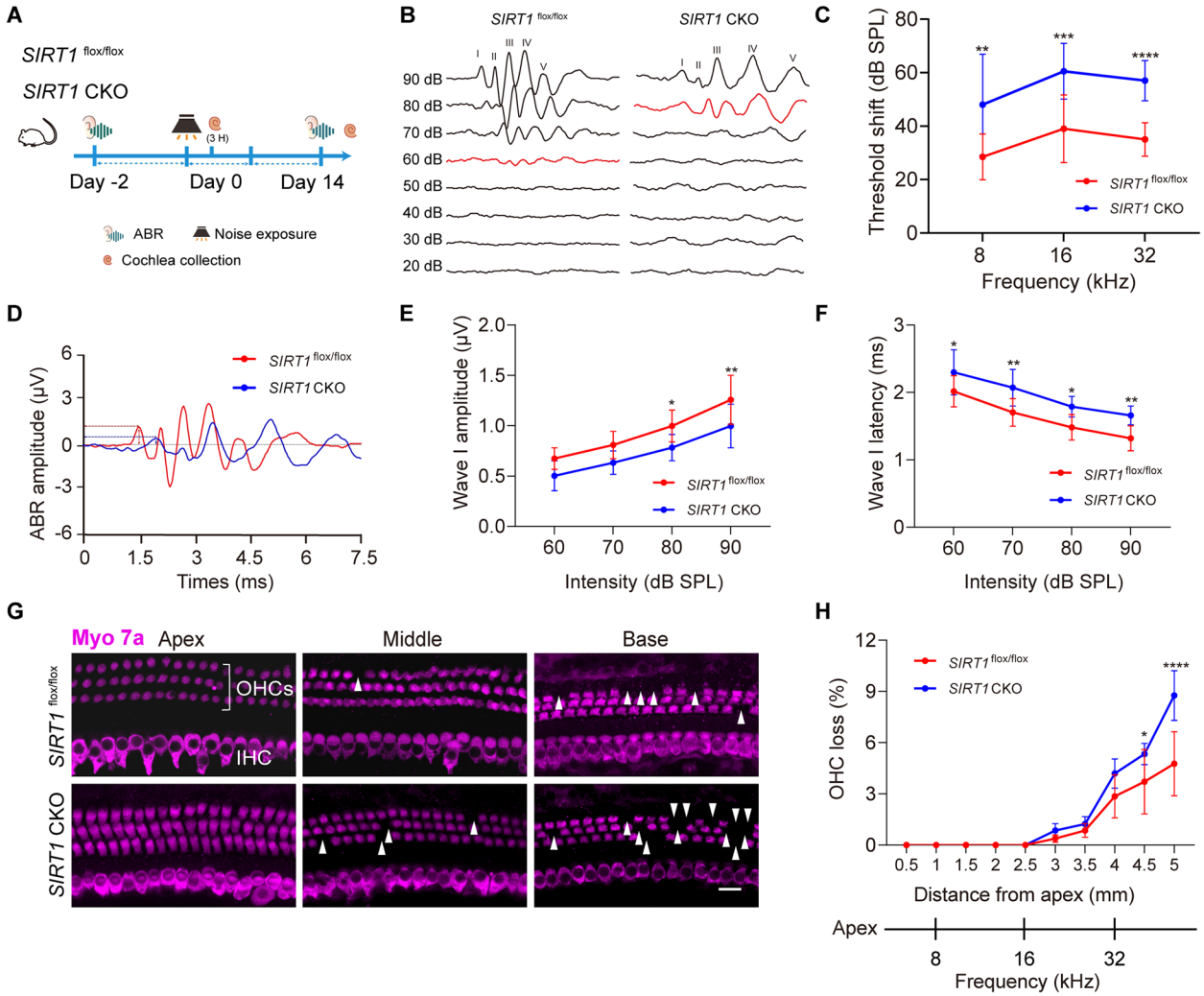

Fig. 2 ABR threshold shifts and morphological changes in OHCs of *SIRT1*$^{flox/flox}$ and *SIRT1* CKO mice after noise exposure. **A** Schematic illustration of the experimental design. **B** Representative ABR waveform in response to stimuli at 8 kHz at different sound levels after noise exposure of *SIRT1*$^{flox/flox}$ and *SIRT1* CKO mice. Red lines indicate thresholds of the ABR responses. **C** ABR threshold shifts after noise exposure in *SIRT1*$^{flox/flox}$ and *SIRT1* CKO mice ($n = 10$, two-way ANOVA with Sidak's multiple comparisons test). **D** Representative ABR waveform in response to stimuli at 8 kHz in 90 dB SPL. **E**, **F***SIRT1* CKO mice demonstrated significantly weaker ABR wave I amplitudes and longer wave I latencies than *SIRT1*.$^{flox/flox}$ mice after noise exposure at 8 kHz in 90 dB SPL to 60 dB SPL ($n = 10$, two-way ANOVA with Sidak's multiple comparisons test). **G** Immunofluorescence images of hair cells (myosin 7a-stained) in the cochlear apex, middle, and basal turns of mice from the two groups. Significant OHC loss was observed in the *SIRT1* CKO group. Scale bar = 20 μm. **H** Hair cells of the entire cochlear spiral were counted and analyzed by the ImageJ software ($n = 4$, two-way ANOVA with Sidak's multiple comparisons test). Data were collected 14 d after exposure. Data are presented as means ± SD. * $p < 0.05$, ** $p < 0.01$, *** $p < 0.001$, **** $p < 0.0001$

terminals, are well-documented [34]. IHCs form specialized ribbon synapses with the dendrites of spiral ganglion neurons (SGNs) and bipolar neurons whose peripheral processes constitute ANFs. These specialized synaptic complexes enable rapid, phase-locked glutamate release through CtBP2-enriched presynaptic machinery, which synchronously activates postsynaptic AMPA receptors (mainly GluA2-harboring subtypes) on SGN dendrites to sustain auditory signaling fidelity [35–37]. We evaluated synaptic integrity by immunostaining for presynaptic CtBP2 and postsynaptic GluA2 markers, combined with neurofilament immunostaining with an anti-NF antibody specific for afferent ANFs (including type I and type II) (Fig. 4A) in four groups: *SIRT1*$^{flox/flox}$, *SIRT1* CKO, *SIRT1*$^{flox/flox}$ + noise, and *SIRT1* CKO + noise. The results showed that under physiological conditions, the numbers of synaptic ribbons and CtBP2 puncta were comparable between the two groups. However, after noise exposure,

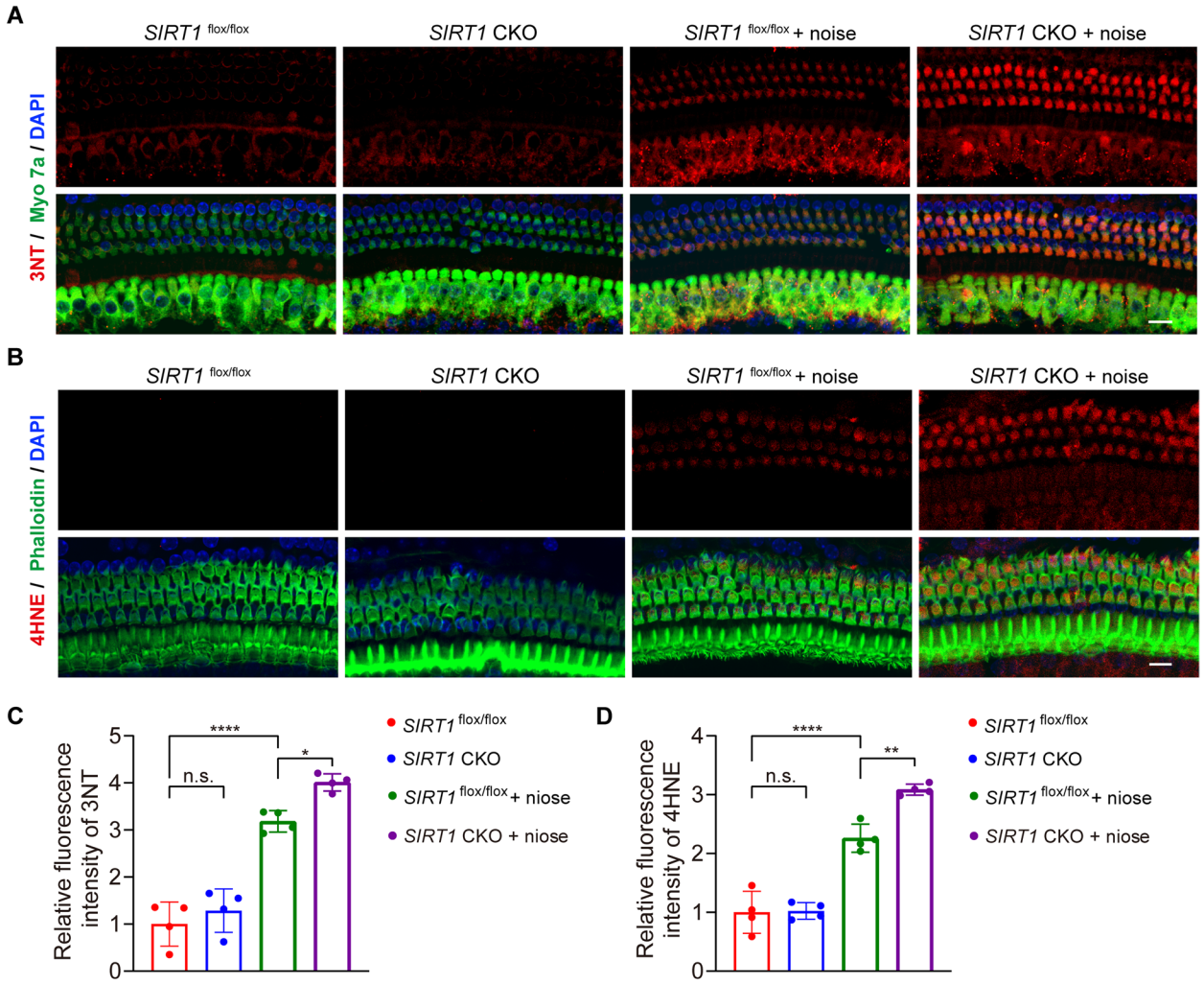

Fig. 3 Noise-induced 3NT and 4HNE accumulation in the hair cells of *SIRT1* CKO mice. **A**, **B** Representative confocal images of the organ of Corti revealing enhanced 3NT (**A**) and 4HNE (**B**) fluorescence signals within the *SIRT1* CKO mouse. Images were taken from the basal turn of mouse cochlea harvested 3 h post-noise exposure. 3NT: 3-nitrotyrosine, 4HNE: 4-hydroxynonenal, scale bar = 20 μm. **C**, **D** Quantification analysis of 3NT and 4HNE fluorescence intensity across groups ($n = 4$, one-way ANOVA with Tukey's post hoc testing). Data are presented as means ± SD. ns: not significant, * $p < 0.05$, ** $p < 0.01$, **** $p < 0.0001$

(See figure on next page.)

Fig. 4 Effect of SIRT1 on synaptopathy and neurite retraction after noise exposure in cochlea. **A** Schematic overview of the organ of Corti: pre- and postsynaptic proteins were stained by CtBP2 (red) and GluA2 (green). Colocalization of CtBP2 and GluA2 labeled synaptic ribbons, whereas individual staining labeled synaptopathy. Neurofilament immunostaining with an anti-NF antibody (orange) specifically marks afferent nerve fibers (including type I and type II). Type I afferent ANFs are associated with IHCs, while type II afferent ANFs are associated with OHCs. CtBP2: C-terminal binding protein 2; GluA2: glutamate ionotropic receptor AMPA type subunit 2; ANFs: auditory nerve fibers. Black dashed boxes indicate the regions where ANF density was calculated. (B, C) Quantification of CtBP2 punctas (**B**) and synaptic ribbons (**C**) assessed 14 days after noise exposure at different turns demonstrated that deletion of SIRT1 alone did not lead to synaptopathology; however, after noise exposure, synaptopathology in *SIRT1* CKO mice was more severe than that in controls ($n = 4$, two-way ANOVA with Sidak's multiple comparisons test). **D** Quantification of type-II ANFs in $SIRT1^{flox/flox}$, *SIRT1* CKO mice, noise-exposed $SIRT1.^{flox/flox}$ and noise-exposed *SIRT1* CKO mice ($n = 4$, two-way ANOVA with Sidak's multiple comparisons test). **E** Fluorescence intensity (mean density) of ANFs (including type I and type II) in a 100-μm wide area from the IHCs to the habenula perforata ($n = 4$, two-way ANOVA with Sidak's multiple comparisons test). **F** Representative confocal images of IHCs and their synaptic ribbons from the 16-kHz region of the four groups. Scale bar = 10 μm. The white dotted circle marked the outline of an IHC and its connected synapses. **G** Representative images of ANFs from the 16-kHz region of the four groups. Neurite retraction (indicated with white arrowheads) and decreased ANF density (indicated with a white square frame) were observed in mice 14 days following noise exposure. Scale bar = 20 μm. Data are presented as means ± SD. * $p < 0.05$, ** $p < 0.01$, *** $p < 0.001$

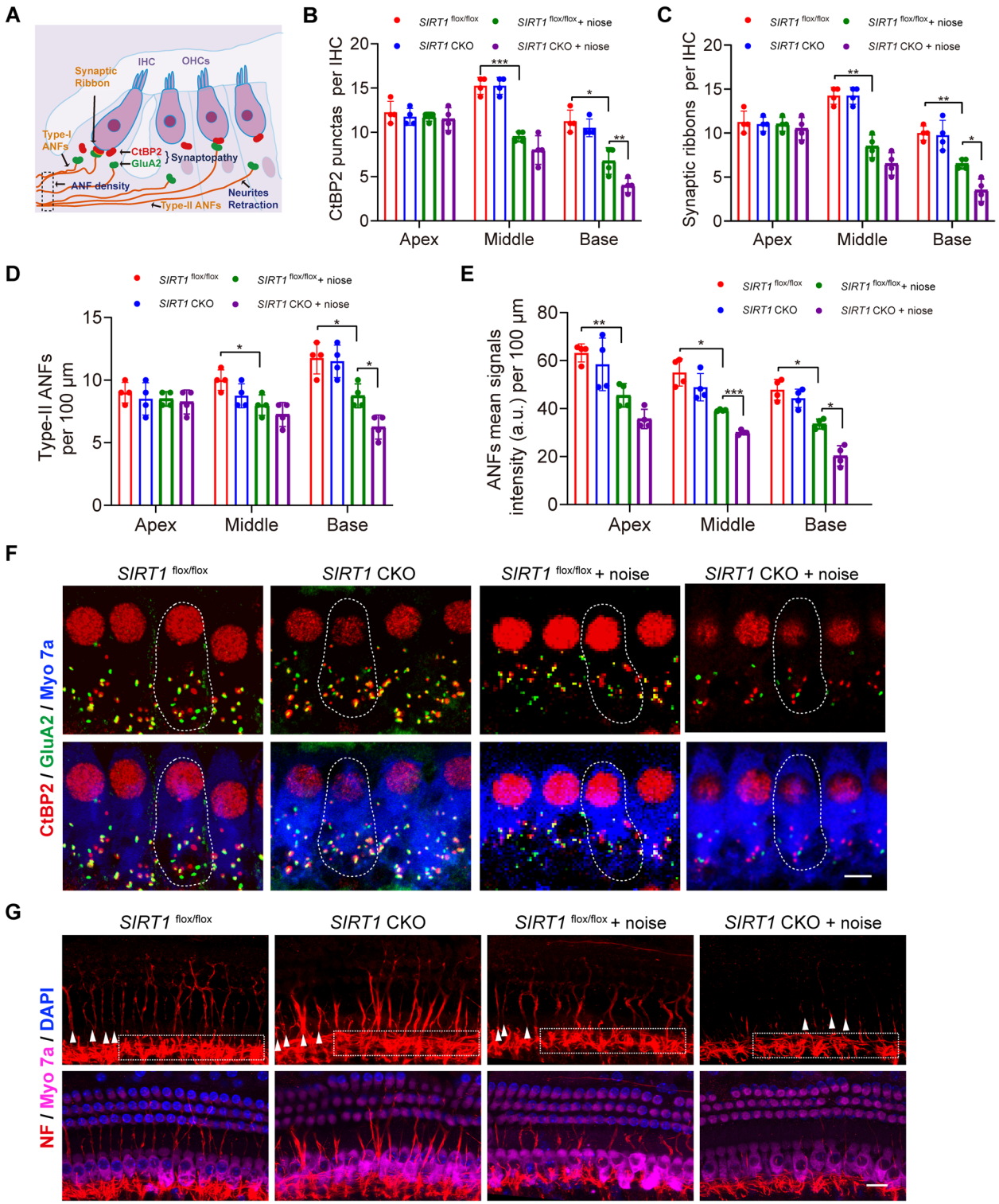

Fig. 4 (See legend on previous page.)

SIRT1 CKO + noise mice exhibited a more severe reduction in synaptic ribbons and CtBP2 puncta than *SIRT1* $^{flox/flox}$ + noise mice, particularly at the basal turn of the cochlea (Fig. 4, B-C, F). Prior to noise exposure, SIRT1 conditional knockout did not affect the number of type II ANFs or the density of ANFs traversing the habenula

perforata. However, following noise exposure, *SIRT1* CKO + noise mice revealed a significantly greater decline in type II ANFs counts than did *SIRT1* $^{flox/flox}$ + noise mice, particularly in the middle and basal turns of the cochlea (Fig. 4, D, G). Furthermore, the density of ANFs passing through the habenula perforata in the apical, middle, and basal turns of the cochlea was more severely reduced in *SIRT1* CKO + noise mice than in *SIRT1* $^{flox/flox}$ + noise mice following noise exposure (Fig. 4E). Notably, in the apical region, although the numbers of type II ANFs remained stable after noise exposure (Fig. 4D), the mean signal intensity, which included contributions from both type I and II afferent fibers, demonstrated a significant reduction. This discrepancy likely stems from the inability of the stable density of type II fibers (constituting 5% of the total innervation) to functionally compensate for the substantial degeneration of the predominant type I fibers (representing 95% of the total innervation). This disproportional change aligns mechanistically with previous observations of auditory neuropathy [26].

These findings indicate that SIRT1 deficiency exacerbates noise-induced synaptic degeneration and ANF retraction, which may account for the heightened ABR threshold shift noted in *SIRT1* CKO mice. Despite the significant increase in the ABR threshold, the rate of OHC loss remained relatively modest, indicating that synaptic and neural damage preceded substantial hair cell loss in this model.

AAV-mediated SIRT1 overexpression protects against NIHL and hair cell loss

To further verify the causal relationship between SIRT1 and NIHL, wild-type C57BL/6 J mice were transfected with AAV2/anc80L65 carrying SIRT1-expressing plasmids to overexpress SIRT1 (AAV-SIRT1) and an AAV vehicle as a negative control (AAV-CTRL) (Fig. 5A), based on the high efficiency of AAV2/anc80L65 vectors in infecting IHCs and OHCs [38]. AAV-CTRL and AAV-SIRT1 were injected into the left ear of postnatal day 2–3 (P2-3) mice via the PSC (Supplemental Fig. 4A). Auditory function was evaluated 4 weeks post-injection using ABR testing. Hearing thresholds at 8, 16, and 32 kHz were measured, indicating no significant difference between AAV-CTRL and AAV-SIRT1 mice (Supplemental Fig. 4B). Immunofluorescence analysis of hair cells confirmed a 2.71-fold increase in SIRT1 expression in AAV-SIRT1 mice relative to AAV-CTRL mice (Supplemental Fig. 4, C-D). GFP-positive cells were counted to evaluate the transfection efficiency, demonstrating no significant differences between the two groups (Supplemental Fig. 4E). Infection rates reached 100% along the entire cochlear spiral in both groups. The transfection rates of OHCs in the apical, middle, and basal turns were 56.19%, 80.71%, and 87.5% in the AAV-CTRL group and 54.55%, 85.52%, and 88.61% in the AAV-SIRT1 group, respectively. These results demonstrated the effective overexpression of SIRT1 in cochlear sensory cells, providing a robust platform for further functional studies.

At 5 weeks of age, AAV-SIRT1 and AAV-CTRL mice were exposed to 108 dB SPL noise for 2 h, and hearing thresholds were evaluated 14 days post-exposure. AAV-SIRT1 mice exhibited a significant reduction in threshold shifts, particularly at 16 and 32 kHz, wherein the mean threshold shifts were reduced by 24.29 dB compared with AAV-CTRL mice (Fig. 5, B-C). The mean threshold shift at 8 kHz was reduced by 14.29 dB, although this difference was not statistically significant.

Furthermore, SIRT1 overexpression mitigated the noise-induced deficits in ABR wave I amplitude and latency at 8 kHz (Fig. 5, D-F). Immunohistochemical analysis using myosin VIIa staining revealed that AAV-SIRT1 significantly reduced the OHC loss along the cochlear spiral following noise exposure (Fig. 5H). In AAV-CTRL mice, OHC loss began 3 mm from the cochlear apex and reached 5.905% at 5 mm, whereas in AAV-SIRT1 mice, OHC loss was reduced by 3.524% at 5 mm (Fig. 5G). These findings highlight the protective effects of SIRT1 overexpression against noise-induced hearing and cochlear OHC loss.

SIRT1 overexpression alleviates noise-induced oxidative stress, synaptopathy, and neurite degeneration in hair cells

To further investigate the role of SIRT1 in mitigating oxidative stress, we examined the levels of 3NT and 4HNE, which are markers of oxidative damage, in cochlear hair cells from the four groups: AAV-CTRL, AAV-SIRT1, AAV-CTRL + noise, and AAV-SIRT1 + noise. The fluorescence intensity of 3NT and 4HNE increased significantly in hair cells of the AAV-CTRL + noise group but decreased significantly in the AAV-SIRT1 + noise group (Supplemental Fig. 5, A-B). Additionally, there was no difference in the number of CtBP2-labeled synapses in the apex, middle, and basal turns of AAV-CTRL and AAV-SIRT1 hair cells under baseline conditions. Additionally, noise exposure led to a reduction in CtBP2-labeled synapses in the middle and basal turns of both AAV-CTRL + and AAV-SIRT1 + noise mice, although this decrease was less pronounced in AAV-SIRT1 mice (Fig. 6, A-B). Furthermore, SIRT1 overexpression considerably alleviated the noise-induced reductions in type II ANF density, particularly in the middle and basal turns (Fig. 6, C-D). The ANF fluorescence intensity in the apex, middle, and basal turns was also higher in AAV-SIRT1 + noise mice than in AAV-CTRL + noise mice (Fig. 6E). Altogether, these results indicated that SIRT1 overexpression effectively reduced noise-induced oxidative stress and preserved synaptic and neural integrity in the cochlea.

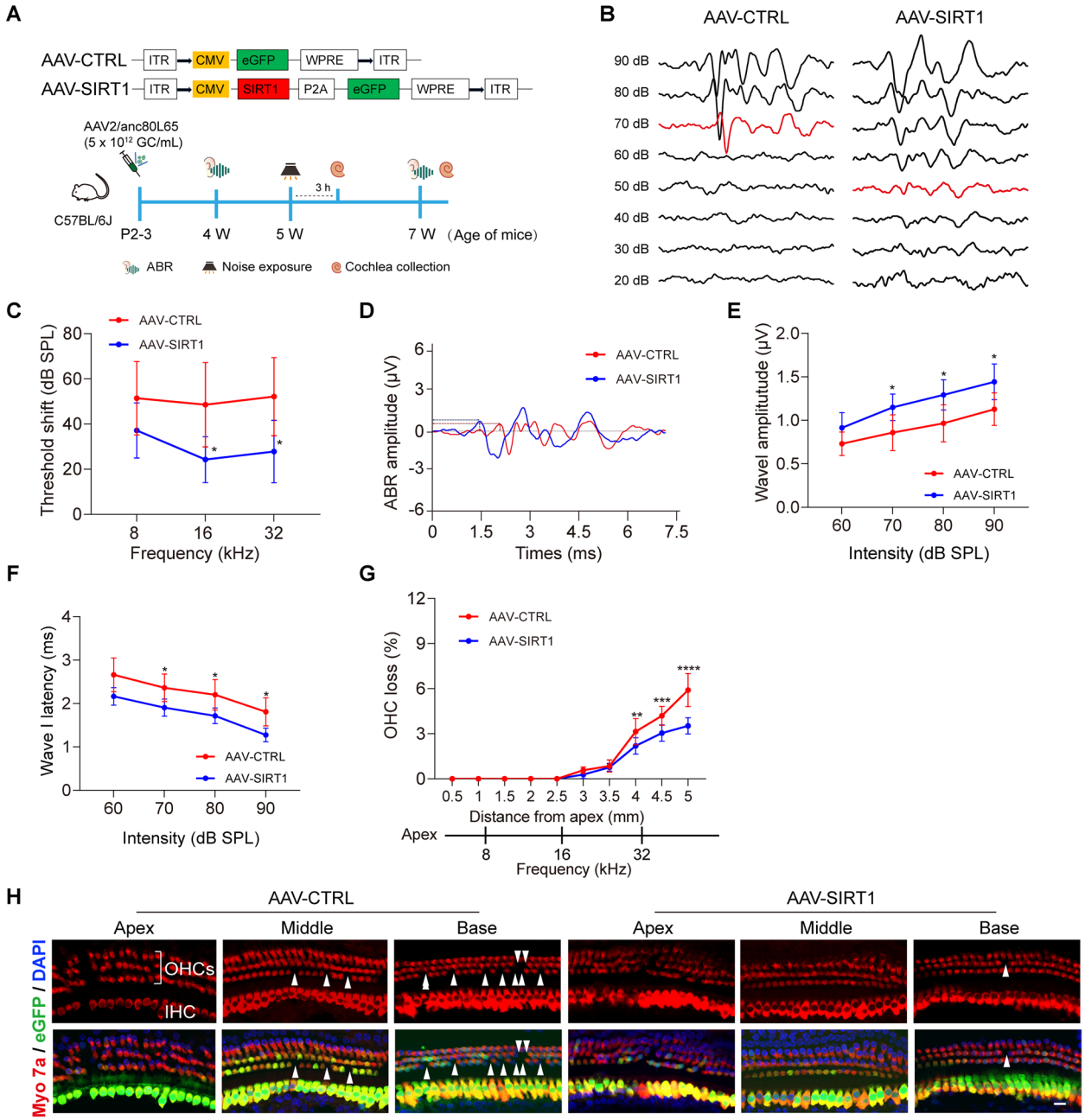

Fig. 5 AAV-mediated SIRT1 overexpression protected against noise-induced OHC loss and hearing loss in C57BL/6 J mice. **A** Diagram illustrating the AAV vector plasmid and the experimental timeline in C57BL/6 J mice. eGFP: enhanced green fluorescent protein; AAV-CTRL: AAV2/anc80L65-ITR-CMV-eGFP-WPRE-ITR; and AAV-SIRT1: AAV2/anc80L65-ITR-CMV-SIRT1-P2A-eGFP-WPRE- ITR. **B** Representative ABR waveform in response to stimuli at 8 kHz at different sound levels after noise exposure of AAV-CTRL and AAV-SIRT1 mice. Red lines indicate thresholds of the ABR responses. **C** Noise-induced auditory threshold shifts were considerably reduced in AAV-SIRT1 mice compared to AAV-CTRL mice measured 14 days after noise exposure for each individual mouse ($n = 7$, two-way ANOVA with Sidak's multiple comparisons test). **D** Representative ABR waveform in response to stimuli at 8 kHz in 90 dB SPL. **E**, **F** AAV-SIRT1 mice revealed significantly greater ABR wave I amplitudes (**E**) and shorter wave I latencies (**F**) than AAV-CTRL mice after noise exposure ($n = 7$, two-way ANOVA with Sidak's multiple comparisons test). **G** OHCs of the entire cochlear spiral were counted and analyzed using the ImageJ software ($n = 4$, two-way ANOVA with Sidak's multiple comparisons test). **F** Immunofluorescence images of HCs in the cochlear apex, middle, and basal turns mice from the two groups. Arrowheads mark areas of lost OHCs. Scale bar = 20 μm. Data are presented as means ± SD. * $p < 0.05$, *** $p < 0.001$, **** $p < 0.0001$

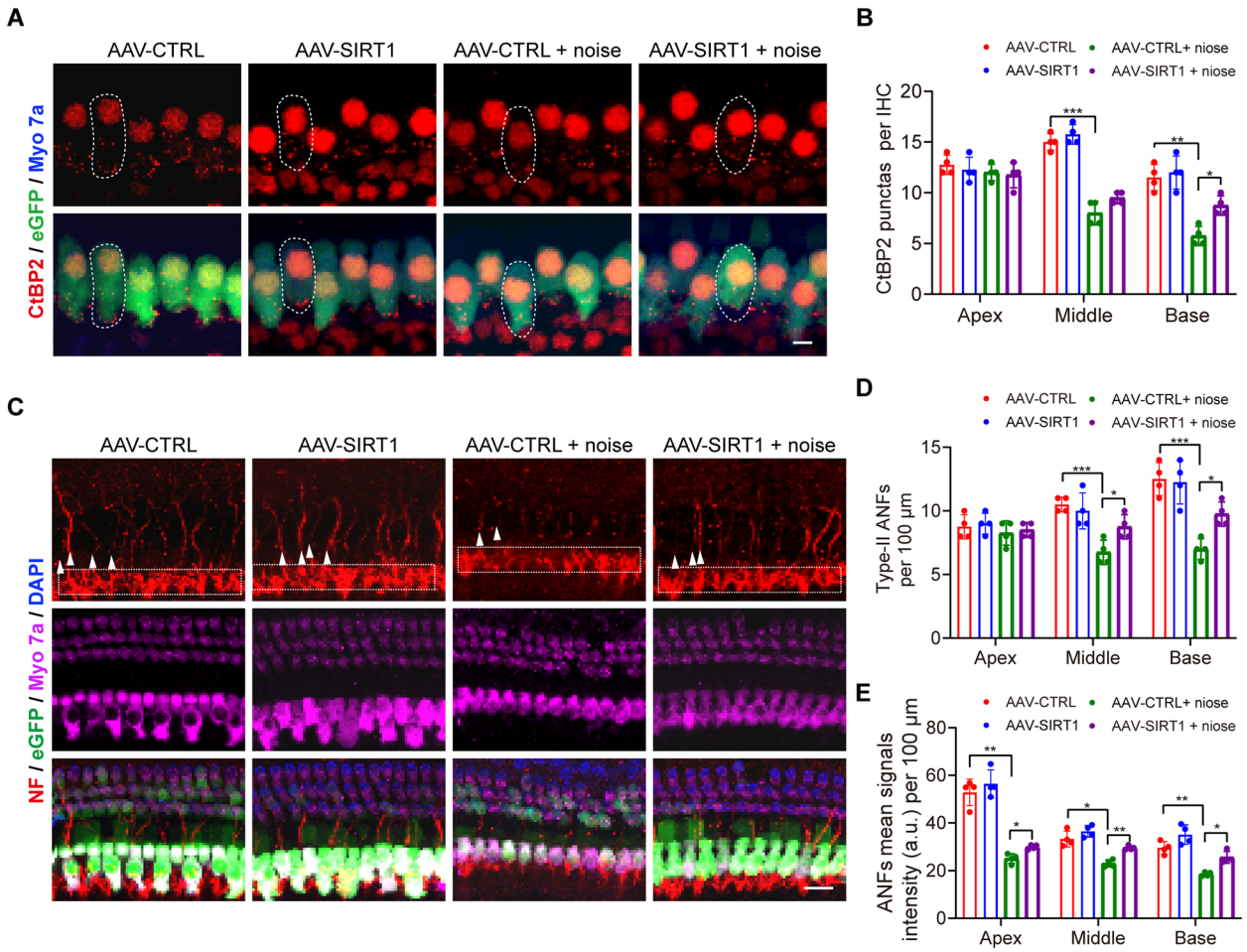

Fig. 6 AAV-mediated SIRT1 overexpression significantly protected against synaptopathy and neurite retraction. **A** Representative immunostaining of CtBP2 punctas in 22-kHz region. CtBP2: C-terminal binding protein 2. Scale bar = 10 μm. **B** Counts of CtBP2 punctas across groups ($n = 4$ for each group, two-way ANOVA with Sidak's multiple comparisons test). **C** Representative confocal images of immunolabeling for auditory nerve fibers (ANFs) by anti-NF antibody (red) from the 16-kHz region of the four groups. Neurites retraction (indicated with white arrowheads) and decreased-ANFs density (indicated with a white square frame) were observed in mice 14 days following noise exposure. Scale bar = 20 μm. **D** Quantification of type-II ANFs ($n = 4$, two-way ANOVA with Sidak's multiple comparisons test). **E** Fluorescence intensity (mean density) of ANFs (including type I and type II) in a 100-μm wide area from the IHCs to the habenula perforata ($n = 4$, two-way ANOVA with Sidak's multiple comparisons test). Data are presented as means ± SD. * $p < 0.05$, ** $p < 0.01$, *** $p < 0.001$

Loss of SIRT1 alters glucose metabolism, antioxidant pathways, and mitochondrial function in cochlea following noise exposure

To investigate the mechanism by which SIRT1 mitigates NIHL, we conducted transcriptomic analysis of cochlear tissues from *SIRT1* $^{flox/flox}$ and *SIRT1* CKO mice following noise exposure. Principal component analysis (PCA) of all differentially expressed genes (DEGs) revealed that *SIRT1* CKO mice exhibited profound alterations in the cochlear transcriptome (Supplemental Fig. 7A). As illustrated in the volcano plot, 298 DEGs were upregulated and 859 were downregulated in the *SIRT1* CKO group compared to the control group (Supplemental Fig. 7B). Notably, several genes involved in glycolysis/gluconeogenesis (GNG) pathways, such as alcohol dehydrogenase 7 (*Adh7*) and glucokinase (*Gck*), and genes related to antioxidant defense, including gamma-glutamyltransferase 6 (*Ggt6*), glutathione S-transferase pi 3 (*Gstp3*), and microsomal glutathione S-transferase 2 (*Mgst2*), were downregulated in response to SIRT1 deletion (Fig. 7A). Additionally, genes implicated in the AMPK signaling pathway, including cystic fibrosis transmembrane conductance regulator (*Cftr*) and protein kinase AMP-activated non-catalytic subunit gamma 3 (*Prkag3*), along with those associated with oxidative phosphorylation, such as cytochrome c oxidase subunit 6a2 (*Cox6a2*) and ATPase H^+ transporting v1 subunit g3 (*Atp6v1g3*), were significantly downregulated. The mTOR signaling pathway was similarly affected, with the downregulation of protein kinase C gamma (*Prkcg*), tumor necrosis factor

(*Tnf*), and wnt family member 10b (*Wnt10b*) (Fig. 7A). The differential expression patterns noted via RNA-Seq were corroborated by qRT-PCR, confirming that *SIRT1* CKO substantially affects glucose metabolism, antioxidant capacity, mitochondrial function, and key signaling pathways within the cochleae (Fig. 7, B-F).

To further explore these metabolic alterations, glucose metabolomic analysis was conducted on the cochlear tissues from *SIRT1* $^{flox/flox}$ and *SIRT1* CKO mice post-noise exposure. A clear separation between the two groups was observed in the PCA plot (Supplemental Fig. 7C). Metabolites involved in glycolysis/GNG (gluconeogenesis) and the tricarboxylic acid (TCA) cycle exhibited an overall increase in the *SIRT1* CKO group, with statistically significant elevations in lactate, α-ketoglutarate (α-KG), and succinate levels (Fig. 7, G-H). Additionally, ATP content was reduced in *SIRT1* CKO mice compared to that in controls (Fig. 7I).

SIRT1 overexpression mitigates oxidative stress and mitochondrial dysfunction in HEI-OC1 cells exposed to H_2O_2

The AMPK signaling pathway, which plays a critical role in regulating energy metabolism and oxidative stress responses, appeared to be significantly influenced by SIRT1 in our NIHL mouse model. Thus, we propose that SIRT1 modulates glucose metabolism and antioxidant defenses, at least in part, through regulation of the AMPK pathway upon noise exposure. We used an in vitro model to further elucidate the molecular mechanisms by which SIRT1 protects the mitochondria from oxidative stress and preserves mitochondrial function. As previously reported, oxidative stress was induced using H_2O_2 to simulate the effects of noise exposure in HEI-OC1 cells [5, 39]. In our study, HEI-OC1 cells were infected with SIRT1-overexpressing lentivirus (SIRT1-OE) or lentivirus vehicle as a negative control (NC-OE), and fluorescence microscopy imaging, qRT-PCR, and western blotting were used to confirm SIRT1-overexpression (Supplemental Fig. 6, A-D). NC-OE and SIRT1-OE cells were treated with various concentrations of hydrogen peroxide (H_2O_2) to induce oxidative stress (Fig. 8A). Upon exposure to 2.5, 5, and 7.5 mM of H_2O_2, the SIRT1-OE group demonstrated greater resistance to oxidative stress-induced damage compared to the NC-OE group, as CCK-8 assays revealed that cell viability in NC-OE cells decreased by 44% and 59%, following exposure to 5 mM and 7.5 mM H_2O_2, while SIRT1-OE cells rescued 11% and 12% of the cell viability (Fig. 8B). For subsequent experiments, 5 mM H_2O_2 was used to simulate oxidative stress conditions. Moreover, levels of mitochondrial oxygen species (mtROS) were quantified by MitoSOX staining, which revealed a two-fold increase in MitoSOX fluorescence in NC-OE cells following H_2O_2 exposure, whereas SIRT1-OE cells exhibited significantly reduced mtROS levels (Fig. 8, C-D). ATP assays demonstrated that the intracellular ATP levels were sharply reduced by H_2O_2 treatment; however, SIRT1 overexpression mitigated this effect (Fig. 8E). Furthermore, qRT-PCR analysis revealed that H_2O_2-induced reductions in the mRNA levels of genes involved in mitochondrial respiratory complexes, such as mitochondrially encoded cytochrome c oxidase I (mt*Co1*), succinate dehydrogenase complex subunit a (*Sdha*), ubiquinol-cytochrome c reductase core protein II (*Uqcrc2*) mitochondrially encoded ATP synthase membrane subunit 6 (*mtAtp6*)), and sirtuin 3 (*Sirt3*), were partially rescued by SIRT1 overexpression (Fig. 8F). These results show that H_2O_2-induced oxidative stress in cells leads to decreased viability, increased mtROS, reduced ATP levels, and downregulation of oxidative phosphorylation (OxPhos) genes, consistent with the changes induced by noise exposure in vivo. This not only confirms the protective effect of SIRT1 in vitro but also indicates that cellular models can effectively simulate in vivo responses to a certain extent, providing a valuable tool for mechanistic research.

SIRT1 preserves mitochondrial function through AMPK activation

We examined AMPK activation following noise exposure in vivo and in vitro to explore the role of AMPK in the SIRT1-mediated protection of mitochondrial homeostasis and function. Immunofluorescence analysis revealed that p-AMPK levels were lower in *SIRT1* CKO mice compared to *SIRT1* $^{flox/flox}$ mice following noise exposure (Fig. 9A, B). CC, an AMPK inhibitor, blocked AMPK

(See figure on next page.)

Fig. 7 Effect of *SIRT1* CKO on glucose metabolism, antioxidant pathways, and mitochondrial function in cochlea following noise exposure. **A** Heatmap showing *SIRT1* CKO-downregulated genes related to glycolysis/gluconeogenesis (GNG), glutathione metabolism, AMPK signaling pathway, oxidative phosphorylation, and mTOR signaling pathway, based on the RNA sequencing analysis ($n = 5$ in the *SIRT1* $^{flox/flox}$ group and $n = 6$ in the *SIRT1* CKO group). **B**-**F** Relative mRNA level of genes related to glycolysis/GNG (*Adh7* and *Gck*), glutathione metabolism (*Ggt6*, *Gstp3*, and *Mgst2*), AMPK signaling pathway (*Cftr* and *Prkag3*), oxidative phosphorylation (*Cox6a2* and *Atp6v1g3*), and mTOR signaling pathway (*Prkcg*, *Tnf* and *Wnt10b*), measured by qRT-PCR ($n = 3$, unpaired 2-tailed Student's *t* test). **G** Histograms of data from (**H**) showing the levels of lactate, α-ketoglutarate, and succinate ($n = 4$, unpaired 2-tailed Student's *t* test). **H** Heatmap showing cochlea metabolites from glycolysis/GNG and TCA cycle ($n = 4$ in each group). **I** Measurement of the content of ATP in the group of *SIRT1*.$^{flox/flox}$ and *SIRT1* CKO after noise exposure ($n = 3$, unpaired 2-tailed Student's *t* test). Data are presented as means ± SD. ns: not significant, * $p < 0.05$, ** $p < 0.01$

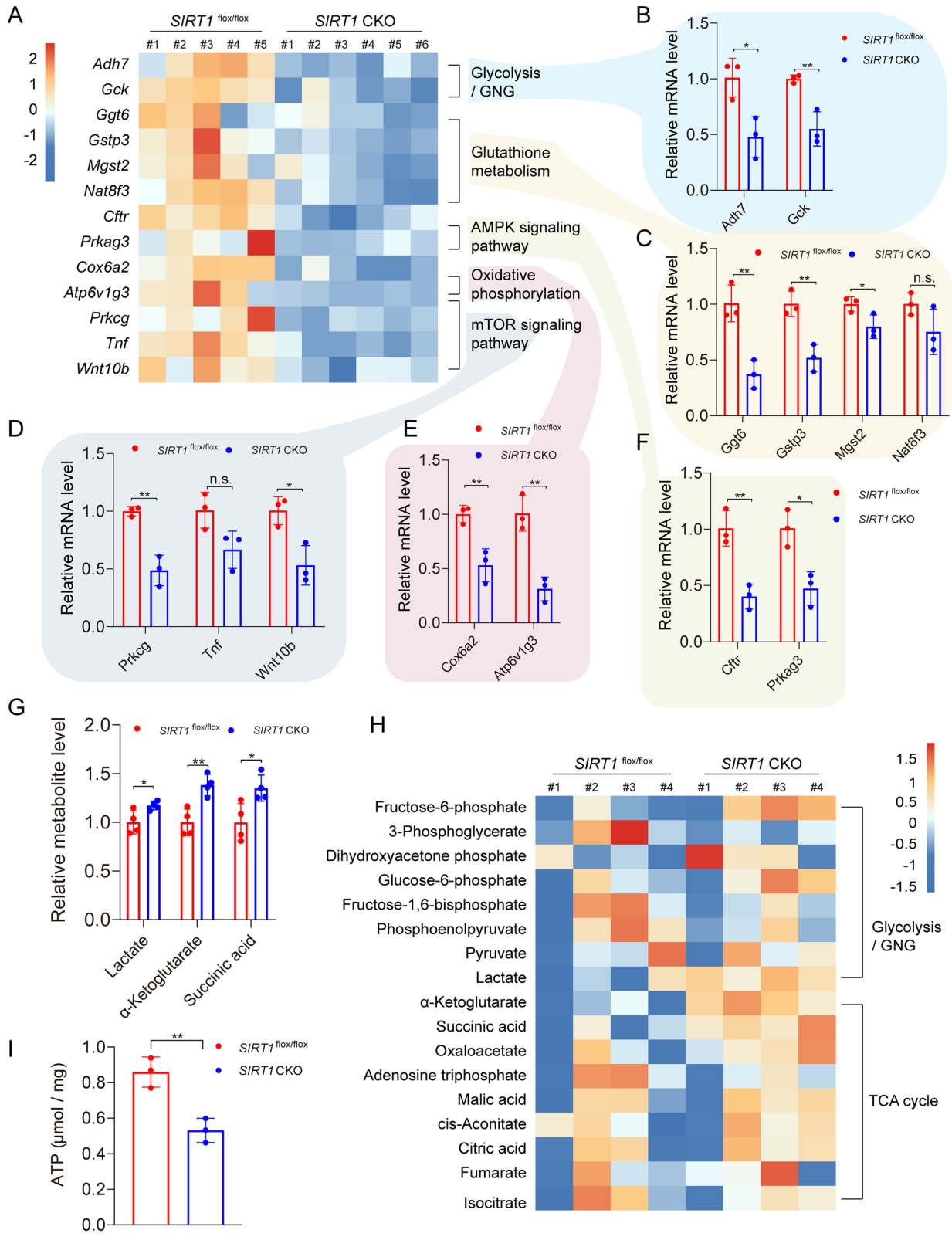

Fig. 7 (See legend on previous page.)

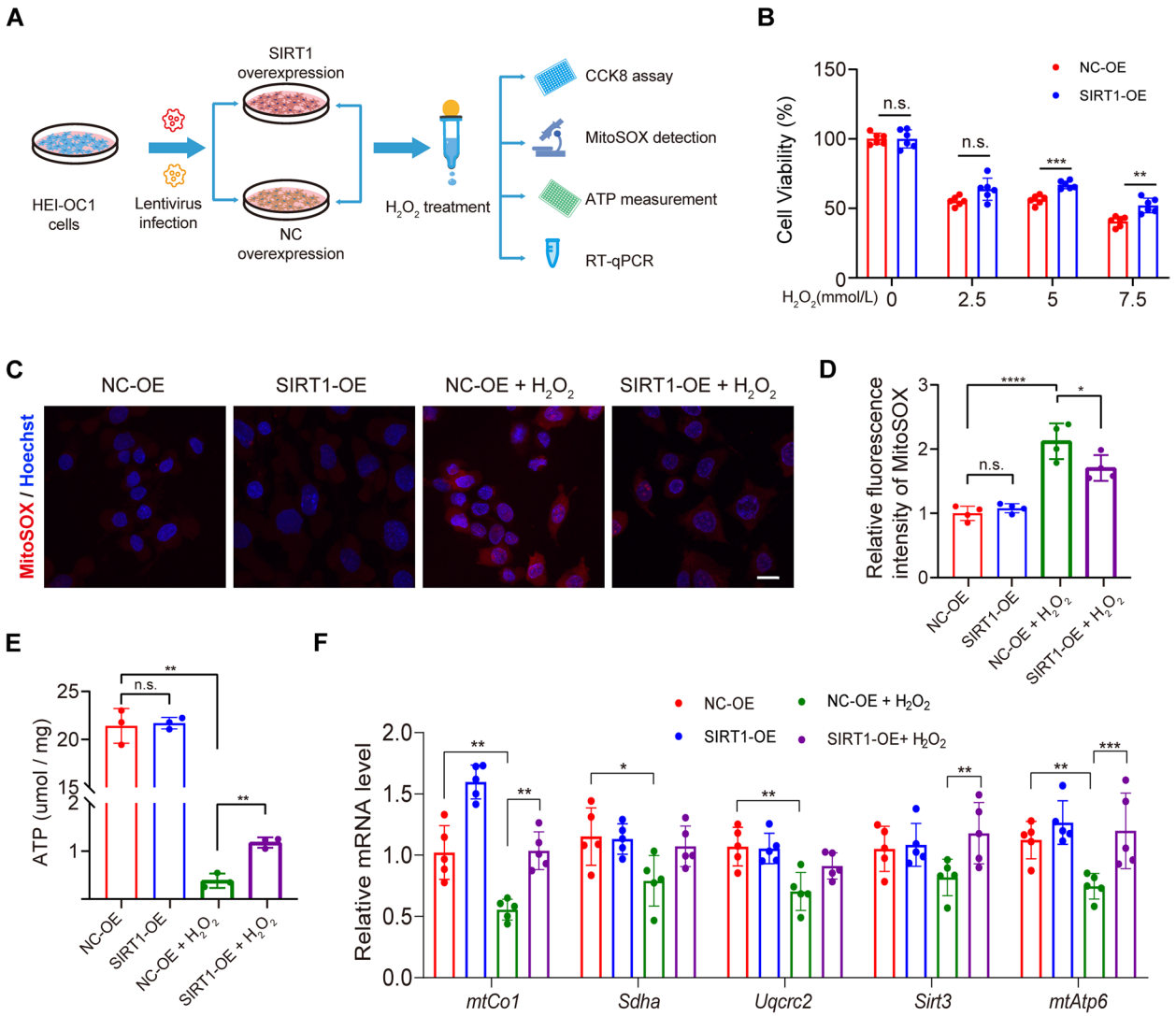

Fig. 8 Overexpression of SIRT1 mediated by lentivirus reduced hydrogen peroxide-induced mitochondrial dysfunction in vitro. **A** Schematic diagram of the workflow. **B** Effects of different concentrations of H_2O_2 on the cell viability of the NC-OE and SIRT1-OE groups ($n=6$, two-way ANOVA with Sidak's multiple comparisons test). OE: overexpression. **C** Representative immunofluorescence images of the MitoSOX (red). Cell nuclei were stained with Hoechst 33,342 (blue). Scale bar = 20 μm. **D** Quantification of the relative immunofluorescence of the MitoSOX ($n=4$, one-way ANOVA with Tukey's post hoc testing). **E** Measurement of the content of ATP in the group of NC-OE, SIRT1-OE groups, NC-OE + H_2O_2, SIRT1-OE + H_2O_2 ($n=3$, one-way ANOVA with Tukey's post hoc testing). The concentration of H_2O_2 was 5 mM. (F) Relative mRNA levels of mitochondrial OxPhos function (*mtCo1*, *Sdha*, *Uqcrc2*, and *mtAtp6*) and *Sirt3* in four groups ($n=5$, one-way ANOVA with Tukey's post hoc testing). Data are presented as means ± SD. * $p<0.05$, ** $p<0.01$, *** $p<0.001$, **** $p<0.0001$

phosphorylation in HEI-OC1 cells. Under H_2O_2-induced oxidative stress, SIRT1 overexpression preserved cell viability, mitigated mitochondrial reactive oxygen species production, and sustained intracellular ATP levels. However, these protective effects were abolished in the presence of CC (Fig. 9, C-H). Collectively, these findings suggested that SIRT1 modulates energy metabolism and oxidative stress responses, at least in part, via AMPK activation in cochlear hair cells under oxidative stress.

Discussion

In the present study, we found that the levels and activity of SIRT1 decreased in the cochlea after exposure to noise. SIRT1 knockout exacerbated cochlear damage and NIHL, whereas SIRT1 overexpression alleviated these effects. Transcriptomic and metabolomic analyses indicated that SIRT1 deficiency affects mitochondrial function and glucose metabolism in the cochlea. Further in vitro experiments suggested that the protective effect

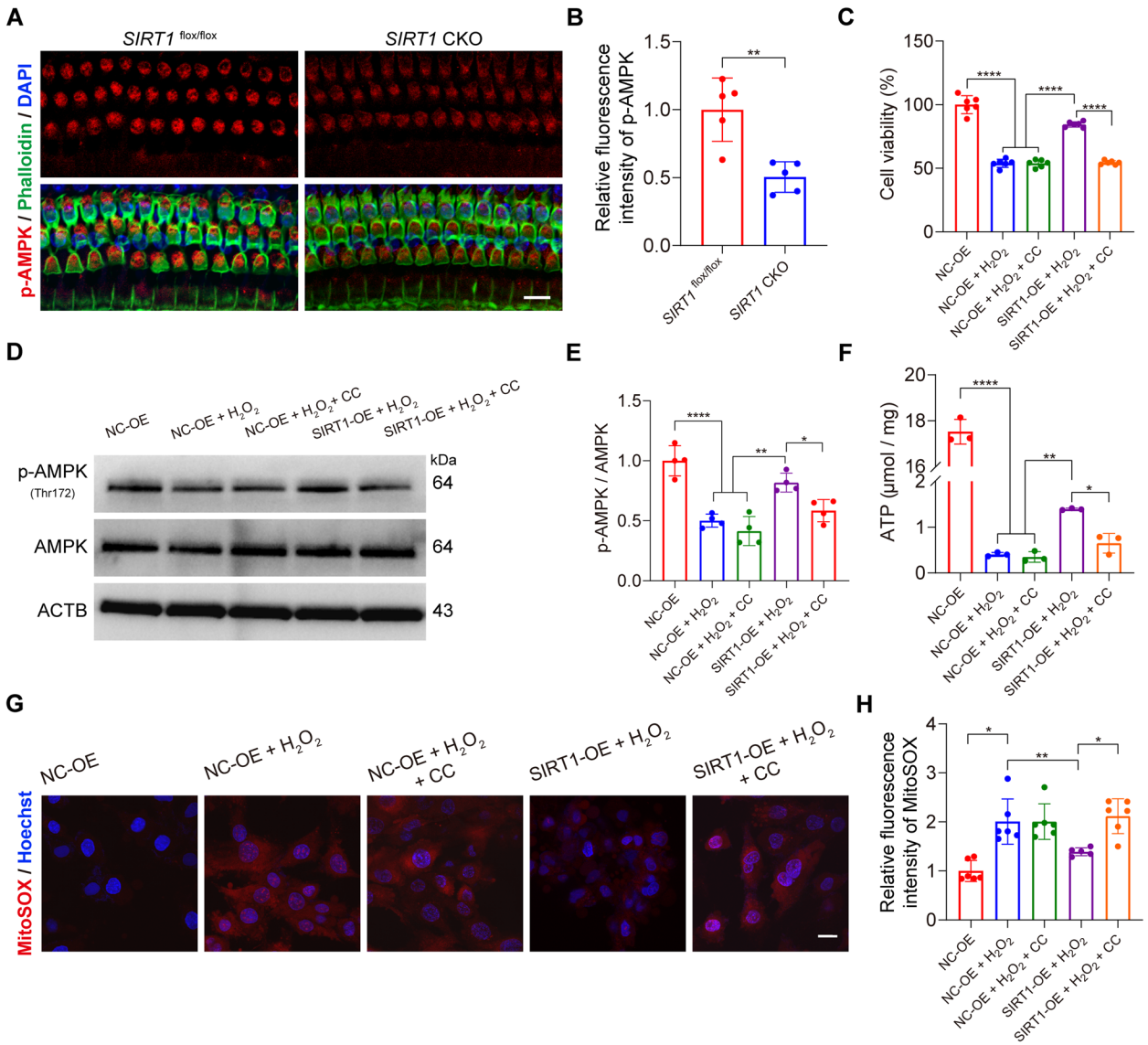

Fig. 9 SIRT1 preserved mitochondrial function through AMPK activation. **A** Representative confocal images demonstrating decreased p-AMPK fluorescence signals within the *SIRT1* CKO mouse. Images were taken from the basal turn of mouse cochlea harvested 1 h post-noise exposure. Scale bar = 20 μm. **B** Quantification of the fluorescence signals of p-AMPK ($n = 5$, unpaired 2-tailed Student's t test). **C** Quantification of cell viability. HEI-OC1 cells were divided into five groups: NE-OE (served as the control group), NE-OE + H_2O_2 (5 mM H_2O_2 treatment for 30 min), NE-OE + H_2O_2 + CC (10-μM compound C pretreatment for 2 h, then 5 mM H_2O_2 treatment for 30 min), SIRT1-OE + H_2O_2 and SIRT1-OE + H_2O_2 + CC ($n = 6$, one-way ANOVA with Tukey's post hoc testing). **D**, **E** Western blot analysis (**D**) and densitometric quantification (**E**) of p-AMPK(Thr172) and AMPK of the five groups ($n = 4$ one-way ANOVA with Tukey's post hoc testing). (**F**) ATP levels of the five groups ($n = 3$, one-way ANOVA with Tukey's post hoc testing). **G**, **H** Representative confocal images (**G**) and fluorescence signal quantification (**H**) of MitoSOX of the five groups ($n = 6$, one-way ANOVA with Tamhane's T2 post hoc testing). Data are presented as means ± SD. * $p < 0.05$, ** $p < 0.01$, *** $p < 0.001$, **** $p < 0.0001$

of SIRT1 was partially mediated by AMPK regulation (Graphical abstract).

We first explored the long-term changes in SIRT1 after noise exposure and found that the decline in SIRT1 expression and activity lasted until the 7th day after noise exposure. These findings align with those of previous studies that identified noise-induced downregulation of SIRT1 [32, 40]. C57BL/6 J mice are widely used as animal models because of their high susceptibility to NIHL [41, 42]. Our findings corroborate those of prior research showing significant hearing loss with relatively minor OHC loss in this model [28, 43]. The limited OHC loss indicates that mechanisms other than direct hair cell death, such as synaptic degeneration, ANF loss, and

mitochondrial dysfunction, play a role in hearing impairment [9, 44]. We observed substantial degeneration of ANFs and marked mitochondrial dysfunction within the cochlea, which was characterized by impaired glucose metabolism and increased mtROS production. These findings align with previous studies suggesting that decreased mitochondrial function, specifically reprogramming glucose metabolism, and increased oxidative stress could underlie impaired responsiveness of hair cells to sound stimuli, ultimately leading to hearing loss [45–47].

Cochlear hair cells require substantial energy to convert sound waves into neural signals, which involves rapid ion exchange and continuous ATP synthesis [48]. This energy demand significantly relies on glucose metabolism to drive ATP production via mitochondrial oxidative phosphorylation and glycolysis [49]. Our previous study demonstrated that glucose supplementation effectively protects cochlear hair cells from oxidative damage and mitigates NIHL [50]. In this study, transcriptomic and metabolomic analyses revealed that SIRT1 conditional knockout significantly negatively affected the respiratory chain, glutathione synthesis, and glucose metabolism in response to noise exposure. This observation is consistent with the known functions of SIRT1 in other organs such as the brain and liver, where it regulates mitochondrial activity and metabolic homeostasis [17, 51, 52]. Reduced mitochondrial function, including decreased respiratory chain efficiency and impaired ATP production, likely contributes to increased ROS levels, oxidative damage, and diminished antioxidant protein synthesis. The accumulation of ROS may also activate apoptotic pathways such as the MAPK and JNK signaling pathways, triggering caspase cascades and leading to programmed cell death [53]. This dysfunction cascade further compromises cellular integrity and energy-dependent physiological functions such as ion channel activity and synaptic transmission [54, 55]. More importantly, energy deficiency impairs $Ca2^{+}$-dependent synaptic vesicle exocytosis at IHC ribbon synapses, directly reducing ANF activation [56].

Notably, our transcriptomic analysis indicated that SIRT1 deletion downregulated key genes involved in glycolysis, oxidative phosphorylation, and antioxidant defense, underscoring the metabolic alterations induced by SIRT1 loss. The involvement of AMPK in the protective role of SIRT1 is significant, although it was not the top-ranked altered pathway. AMPK serves as a master regulator of cellular energy balance and plays a central role in the oxidative stress response [57, 58]. Previous studies have shown that AMPK inhibition increases intracellular cholesterol synthesis and promotes ROS generation [59], and cells lacking AMPK activity exhibit elevated mtROS levels and undergo premature senescence [60]. Conversely, noise-induced ROS overproduction enhanced p-AMPK levels [61]. The apparent discrepancy between these findings may be explained by the early activation of AMPK, which increases ATP stores, thereby protecting hair cells from death and synaptic loss caused by rapid ATP depletion during subsequent intense noise exposure [62]. Our experiments further confirmed that the inhibition of AMPK could offset the protective effects of SIRT1 overexpression, indicating that AMPK mediates the protective role of SIRT1 against oxidative stress and mitochondrial dysfunction in hair cells (Fig. 9). Thus, targeting the SIRT1-AMPK axis may represent a promising strategy for mitigating NIHL by preserving mitochondrial function and enhancing cellular resilience to noise-induced oxidative stress.

Although our study provides evidence of the protective role of SIRT1 in NIHL, several questions remain unanswered. First, the specific signaling pathways or factors responsible for SIRT1 downregulation in the cochlea remain unknown. Previous studies have suggested that oxidative stress and NAD^{+} depletion may play a central role, and noise-induced overproduction of ROS directly impairs SIRT1 activity [20, 32], whereas overactivation of PARP1 under acoustic stress depletes NAD^{+} pools, thereby limiting SIRT1 enzymatic function [63, 64]. Second, although our study quantified OHC loss, we did not perform functional assessments of OHC integrity, such as distortion product otoacoustic emissions (DP-OAEs). Third, although changes in the AMPK pathway were observed upon SIRT1 modulation, the direct relationship between SIRT1 and AMPK in NIHL models requires in vivo experimental confirmation. Moreover, the exact mechanism by which SIRT1 regulates AMPK expression in cochlear hair cells remains unclear. Previous studies suggest that SIRT1 may modulate AMPK through the deacetylation of LKB1, an upstream kinase of AMPK [34, 65–67]. Finally, we did not explore the effects of SIRT1 on other pathophysiological processes implicated in NIHL, such as autophagy.

In conclusion, we demonstrated that SIRT1 mitigates oxidative stress; reduces hair cell loss, synaptopathy, and neurite retraction; and ultimately alleviates NIHL, at least in part, by preserving mitochondrial function through AMPK activation. These findings highlight SIRT1 as a promising therapeutic target for NIHL.

Abbreviations

3NT	3-Nitrotyrosine
4HNE	4-Hydroxynonenal
AAV	Adeno-associated virus
ABR	Auditory brainstem response
AMPK	5′ Adenosine monophosphate-activated protein kinase
ANF	Auditory nerve fiber
CCK-8	Cell counting kit-8

CKO	Conditional knockout
CtBP2	C-terminal binding protein 2
CTRL	Control
eGFP	Enhanced Green fuorescent protein
GluA2	Glutamate ionotropic receptor AMPA type subunit 2
IHC	Inner hair cell
NIHL	Noise-induced hearing loss
OE	Overexpression
OHC	Outer hair cell
PBS	Phosphate buffered saline
PSC	Posterior semicircular canals
ROS	Reactive oxygen species
SIRT1	Sirtuin 1
SPL	Sound pressure level

Supplementary Information

The online version contains supplementary material available at https://doi.org/10.1186/s12964-025-02152-9.

Supplementary Material 1.

Supplementary Material 2.

Supplementary Material 3.

Authors' contributions

Yuelian Luo: conceptualization, methodology, validation, resources, writing–original draft, writing–review, and editing. Haoyang Wu: conceptualization, validation, visualization, writing, review, and editing. Xin Min: formal analysis, investigation, methodology, visualization. Yi Chen: data curation and investigation. Wenting Deng: data curation. Minjun Chen: formal analysis and software. Chuxuan Yang: formal analysis and software. Hao Xiong: conceptualization, funding acquisition, project administration, supervision, writing-review and editing.

Funding

This work was supported by the National Natural Science Foundation of China (Grant No. 82171134), the Natural Science Foundation of Guangdong Province (Grant No. 2023A1515010465), and the Guangdong Provincial People's Hospital Supporting Fund for Talent Program (Grant No. KY012025018).

Declarations

Competing interests

The authors declare no competing interests.

Author details

[1]Department of Otolaryngology, Sun Yat-Sen Memorial Hospital, Sun Yat-Sen University, Guangzhou, China. [2]Department of Otolaryngology, Guangdong Provincial People's Hospital (Guangdong Academy of Medical Sciences), Southern Medical University, Guangzhou, China.

Received: 2 January 2025 Accepted: 11 March 2025
Published online: 02 April 2025

References

1. World Health Organization, Deafness and hearing loss. 2024. https://www.who.int/news-room/fact-sheets/detail/deafness-and-hearing-loss. Accessed 2 Nov 2024.
2. Xu K, Xu B, Gu J, Wang X, Yu D, Chen Y. Intrinsic mechanism and pharmacologic treatments of noise-induced hearing loss. Theranostics. 2023;13:3524. https://doi.org/10.7150/thno.83383.
3. Fernandez KA, Guo D, Micucci S, Gruttola VD, Liberman MC, Kujawa SG. Noise-induced cochlear synaptopathy with and without sensory cell loss. Neuroscience. 2019;427:43. https://doi.org/10.1016/j.neuroscience.2019.11.051.
4. Mukherjee S, Kuroiwa M, Oakden W, Paul BT, Noman A, Chen J, Lin V, Dimitrijevic A, Stanisz G, Le TN. Local magnetic delivery of adeno-associated virus AAV2(quad Y-F)-mediated BDNF gene therapy restores hearing after noise injury. Mol Ther. 2022;30:519–33. https://doi.org/10.1016/j.ymthe.2021.07.013.
5. Chen F, Jiang Q, Xu B, Huang Y, Xu K, Xu X, Yu D, Chen Y, Wang X. Ototoxicity-alleviating and cytoprotective allomelanin nanomedicine for efficient sensorineural hearing loss treatment. ACS Nano. 2024;18:26401–18. https://doi.org/10.1021/acsnano.4c10610.
6. Wu F, Xiong H, Sha S. Noise-induced loss of sensory hair cells is mediated by ROS/AMPKα pathway. Redox Biol. 2019;29: 101406. https://doi.org/10.1016/j.redox.2019.101406.
7. Zhao Z, Han Z, Naveena K, Lei G, Qiu S, Li X, Li T, Shi X, Zhuang W, Li Y, Qiao Y, Liu H. ROS-responsive nanoparticle as a berberine carrier for OHC-targeted therapy of noise-induced hearing loss. ACS Appl Mater Interfaces. 2021;13:7102–14. https://doi.org/10.1021/acsami.0c21151.
8. Wilhelm LP, Ganley IG. Mitochondria and peroxisomes: partners in autophagy. Autophagy. 2023;19:2162–3. https://doi.org/10.1080/15548627.2022.2155368.
9. Baek J-I, Kim Y-R, Lee K-Y, Kim U-K. Mitochondrial redox system: A key target of antioxidant therapy to prevent acquired sensorineural hearing loss. Front Pharmacol. 2023;14: 1176881. https://doi.org/10.3389/fphar.2023.1176881.
10. Madreiter-Sokolowski CT, Thomas C, Ristow M. Interrelation between ROS and Ca2+ in aging and age-related diseases. Redox Biol. 2020;36: 101678. https://doi.org/10.1016/j.redox.2020.101678.
11. Wang AJ, Tang Y, Zhang J, Wang BJ, Xiao M, Lu G, Li J, Liu Q, Guo Y, Gu J. Cardiac SIRT1 ameliorates doxorubicin-induced cardiotoxicity by targeting sestrin 2. Redox biol. 2022;52:102310. https://doi.org/10.1016/j.redox.2022.102310.
12. Bordone L, Cohen D, Robinson A, Motta MC, Van Veen E, Czopik A, Steele AD, Crowe H, Marmor S, Luo J, Gu W, Guarente L. SIRT1 transgenic mice show phenotypes resembling calorie restriction. Aging Cell. 2007;6:759–67. https://doi.org/10.1111/j.1474-9726.2007.00335.x.
13. Yu H, Zhang F, Yan P, Zhang S, Lou Y, Geng Z, Li Z, Zhang Y, Xu Y, Lu Y, Chen C, Wang D, Zhu W, Hu X, Wang J, Zhuang T, Zhang Y, Wu G, Liu J, Zeng C, Pu WT, Sun K, Zhang B. LARP7 protects against heart failure by enhancing mitochondrial biogenesis. Circulation. 2021;143:2007–22. https://doi.org/10.1161/CIRCULATIONAHA.120.050812.
14. Xu W, Yan J, Ocak U, Lenahan C, Shao A, Tang J, Zhang J, Zhang JH. Melanocortin 1 receptor attenuates early brain injury following subarachnoid hemorrhage by controlling mitochondrial metabolism via AMPK/SIRT1/PGC-1α pathway in rats. Theranostics. 2021;11:522–39. https://doi.org/10.7150/thno.49426.
15. Zhao Y, Zhang J, Zheng Y, Zhang Y, Zhang XJ, Wang H, Du Y, Guan J, Wang X, Fu J. NAD+ improves cognitive function and reduces neuroinflammation by ameliorating mitochondrial damage and decreasing ROS production in chronic cerebral hypoperfusion models through Sirt1/PGC-1α pathway. J Neuroinflammation. 2021;18:207. https://doi.org/10.1186/s12974-021-02250-8.
16. A Mengozzi, S Costantino, F Paneni, E Duranti, M Nannipieri, R Mancini, M Lai, V La Rocca, I Puxeddu, L Antonioli, M Fornai, M Ghionzoli, G Georgiopoulos, C Ippolito, N Bernardini, F Ruschitzka, NR Pugliese, S Taddei, A Virdis*, S Masi. Targeting SIRT1 rescues age- and obesity-induced microvascular dysfunction in ex vivo human vessels. Circ Res. 2022;131:476–491. https://doi.org/10.1161/CIRCRESAHA.122.320888.
17. Li Q, Zhang Q, Kim Y-R, Gaddam RR, Jacobs JS, Bachschmid MM, Younis T, Zhu Z, Zingman L, London B, Rauckhorst AJ, Taylor EB, Norris AW, Vikram A, Irani K. Deficiency of endothelial sirtuin1 in mice stimulates skeletal muscle insulin sensitivity by modifying the secretome. Nat Commun. 2023;14:5595. https://doi.org/10.1038/s41467-023-41351-1.
18. Jiang T, Qin T, Gao P, Tao Z, Wang X, Wu M, Gu J, Chu B, Zheng Z, Yi J, Xu T, Huang Y, Liu H, Zhao S, Ren Y, Chen J, Yin G. SIRT1 attenuates blood-spinal cord barrier disruption after spinal cord injury by deacetylating p66Shc. Redox Biol. 2023;60: 102615. https://doi.org/10.1016/j.redox.2023.102615.
19. Yin X, Li Y, Fan X, Huang F, Qiu Y, Zhao C, Zhou Z, Gu Q, Xia L, Bao J, Wang X, Liu F, Qian W. SIRT1 deficiency increases O-GlcNAcylation of tau, mediating synaptic tauopathy. Mol Psychiatry. 2022;27:4323–34. https://doi.org/10.1038/s41380-022-01689-2.
20. Xiong H, Ou Y, Xu Y, Huang Q, Pang J, Lai L, Zheng Y. Resveratrol promotes recovery of hearing following intense noise exposure by enhancing

cochlear SIRT1 Activity. Audiol Neurotol. 2017;22:303–10. https://doi.org/10.1159/000485312.
21. Xiong H, Dai M, Ou Y, Pang J, Yang H, Huang Q, Chen S, Zhang Z, Xu Y, Cai Y, Liang M, Zhang X, Lai L, Zheng Y. SIRT1 expression in the cochlea and auditory cortex of a mouse model of age-related hearing loss. Exp Gerontol. 2014;51:8–14. https://doi.org/10.1016/j.exger.2013.12.006.
22. Xiong H, Chen S, Lai L, Yang H, Xu Y, Pang J, Su Z, Lin H, Zheng Y. Modulation of miR-34a/SIRT1 signaling protects cochlear hair cells against oxidative stress and delays age-related hearing loss through coordinated regulation of mitophagy and mitochondrial biogenesis. Neurobiol Aging. 2019;79:30–42. https://doi.org/10.1016/j.neurobiolaging.2019.03.013.
23. Zhan T, Xiong H, Pang J, Zhang W, Ye Y, Liang Z, Huang X, He F, Jian B, He W, Gao Y, Min X, Zheng Y, Yang H. Modulation of NAD+ biosynthesis activates SIRT1 and resists cisplatin-induced ototoxicity. Toxicol Lett. 2021;349:115–23. https://doi.org/10.1016/j.toxlet.2021.05.013.
24. Min X, Deng X-H, Lao H, Wu Z-C, Chen Y, Luo Y, Wu H, Wang J, Fu Q-L, Xiong H. BDNF-enriched small extracellular vesicles protect against noise-induced hearing loss in mice. J Control Release. 2023;364:546–61. https://doi.org/10.1016/j.jconrel.2023.11.007.
25. Lao H, Zhu Y, Yang M, Wang L, Tang J, Xiong H. Characteristics of spatial protein expression in the mouse cochlear sensory epithelia: Implications for age-related hearing loss. Hear Res. 2024;446:109006. https://doi.org/10.1016/j.heares.2024.109006.
26. Nieratschker M, Yildiz E, Gerlitz M, Bera S, Gadenstaetter AJ, Kramer A-M, Kwiatkowska M, Mistrik P, Landegger LD, Braun S, Schlingensiepen R, Honeder C, Arnoldner C, Rommelspacher H. A preoperative dose of the pyridoindole AC102 improves the recovery of residual hearing in a gerbil animal model of cochlear implantation. Cell Death Dis. 2024;15:531. https://doi.org/10.1038/s41419-024-06854-9.
27. Hu Y, Ma X. Icariin Treatment Protects Against Gentamicin-Induced Ototoxicity via Activation of the AMPK-SIRT3 Pathway. Front Pharmacol. 2021;12: 620741. https://doi.org/10.3389/fphar.2021.620741.
28. Lee S-Y, Han JJ, Lee S-Y, Jung G, Min HJ, Song J-J, Koo J-W. Outcomes of peptide vaccine GV1001 treatment in a murine model of acute noise-induced hearing loss. Antioxidants (Basel). 2020;9: 112. https://doi.org/10.3390/antiox9020112.
29. Wiwatpanit T, Lorenzen SM, Cantú JA, Foo CZ, Hogan AK, Márquez F, Clancy JC, Schipma MJ, Cheatham MA, Duggan A, García-Añoveros J. Trans-differentiation of outer hair cells into inner hair cells in the absence of INSM1. Nature. 2018;563:691–5. https://doi.org/10.1038/s41586-018-0570-8.
30. Michalski N, Goutman JD, Auclair SM, Boutet de Monvel J, Tertrais M, Emptoz A, Parrin A, Nouaille S, Guillon M, Sachse M, Ciric D, Bahloul A, Hardelin J-P, Sutton RB, Avan P, Krishnakumar SS, Rothman JE, Dulon D, Safieddine S, Petit C. Otoferlin acts as a Ca2+ sensor for vesicle fusion and vesicle pool replenishment at auditory hair cell ribbon synapses. Elife. 2017;6: e31013. https://doi.org/10.7554/eLife.31013.
31. Johnson SL, Olt J, Cho S, von Gersdorff H, Marcotti W. The coupling between Ca2+ channels and the exocytotic Ca2+ sensor at hair cell ribbon synapses varies tonotopically along the mature cochlea. J Neurosci. 2017;37:2471–84. https://doi.org/10.1523/JNEUROSCI.2867-16.2017.
32. Liu Y-H, Jiang Y-H, Li C-C, Chen X-M, Huang L-G, Zhang M, Ruan B, Wang X-C. Involvement of the SIRT1/PGC-1α signaling pathway in noise-induced hidden hearing loss. Front Physiol. 2022;13: 798395. https://doi.org/10.3389/fphys.2022.798395.
33. Matern M, Vijayakumar S, Margulies Z, Milon B, Song Y, Elkon R, Zhang X, Jones SM, Hertzano R. Gfi1Cre mice have early onset progressive hearing loss and induce recombination in numerous inner ear non-hair cells. Sci Rep. 2017;7: 42079. https://doi.org/10.1038/srep42079.
34. Hill K, Yuan H, Wang X, Sha S-H. Noise-induced loss of hair cells and cochlear synaptopathy are mediated by the activation of AMPK. J Neurosci. 2016;36:7497–510. https://doi.org/10.1523/JNEUROSCI.0782-16.2016.
35. Johnson SL, Safieddine S, Mustapha M, Marcotti W. Hair cell afferent synapses: function and dysfunction. Cold Spring Harb Perspect Med. 2019;9: a033175. https://doi.org/10.1101/cshperspect.a033175.
36. Nowak N, Wood M, Glowatzki E, Fuchs P. Prior acoustic trauma alters type ii afferent activity in the mouse cochlea. Eneuro. 2021;8:ENEURO.0383-21.2021. https://doi.org/10.1523/eneuro.0383-21.2021.
37. Karagulyan N, Überegger M, Qi Y, Babai N, Hofer F, Johnson Chacko L, Wang F, Luque M, Glueckert R, Schrott-Fischer A, Hua Y, Moser T, Bandtlow CE. Probing the role of synaptic adhesion molecule RTN4RL2 in setting up cochlear connectivity. bioRxiv. 2024. https://doi.org/10.1101/2024.09.16.613011.
38. Qi J, Zhang L, Tan F, Zhang Y, Zhou Y, Zhang Z, Wang H, Yu C, Jiang L, Liu J, Chen T, Wu L, Zhang S, Sun S, Sun S, Lu L, Wang Q, Chai R. Preclinical efficacy and safety evaluation of AAV-OTOF in DFNB9 mouse model and nonhuman primate. Adv Sci (Weinh). 2023;11: 2306201. https://doi.org/10.1002/advs.202306201.
39. Yang H, Zhu Y, Ye Y, Guan J, Min X, Xiong H. Nitric oxide protects against cochlear hair cell damage and noise-induced hearing loss through glucose metabolic reprogramming. Free Radical Biol Med. 2022;179:229–41. https://doi.org/10.1016/j.freeradbiomed.2021.11.020.
40. Chen X, Liu Y, Ji S, Xue X, Wang L, Zhang M, Chang Y, Wang X. Protective effect of ginsenoside Rd on military aviation noise-induced cochlear hair cell damage in guinea pigs. Environ Sci Pollut Res. 2023;30:23965–81. https://doi.org/10.1007/s11356-022-23504-9.
41. Brown KD, Maqsood S, Huang J-Y, Pan Y, Harkcom W, Li W, Sauve A, Verdin E, Jaffrey SR. Activation of SIRT3 by the NAD+ precursor nicotinamide riboside protects from noise-induced hearing loss. Cell Metab. 2014;20:1059–68. https://doi.org/10.1016/j.cmet.2014.11.003.
42. Liu J, Bai Y, Feng Y, Liu X, Pang B, Zhang S, Jiang M, Chen A, Huang H, Chen Y, Ling J, Mei L. ABCC1 deficiency potentiated noise-induced hearing loss in mice by impairing cochlear antioxidant capacity. Redox Biol. 2024;74: 103218. https://doi.org/10.1016/j.redox.2024.103218.
43. Han S, Du Z, Liu K, Gong S. Nicotinamide riboside protects noise-induced hearing loss by recovering the hair cell ribbon synapses. Neurosci Lett. 2020;725: 134910. https://doi.org/10.1016/j.neulet.2020.134910.
44. Zheng Z, Zeng S, Liu C, Li W, Zhao L, Cai C, Nie G, He Y. The DNA methylation inhibitor RG108 protects against noise-induced hearing loss. Cell Biol Toxicol. 2021;37:751–71. https://doi.org/10.1007/s10565-021-09596-y.
45. Xu J, Jackson CW, Khoury N, Escobar I, Perez-Pinzon MA. Brain SIRT1 Mediates Metabolic Homeostasis and Neuroprotection. Front Endocrinol (Lausanne). 2018;9:702. https://doi.org/10.3389/fendo.2018.00702.
46. Huang Q, Su H, Qi B, Wang Y, Yan K, Wang X, Li X, Zhao D. A SIRT1 activator, ginsenoside Rc, promotes energy metabolism in cardiomyocytes and neurons. J Am Chem Soc. 2021;143:1416–27. https://doi.org/10.1021/jacs.0c10836.
47. Zhang J, Gong T, Chen P, Zhu J, Huang S, Li Y, Li G, Zhang Q, Duan M, Song Q, Yang J, Hou S. Connexin30-deficient mice increase susceptibility to noise via redox and lactate imbalances. Free Radical Biol Med. 2024;225:641–53. https://doi.org/10.1016/j.freeradbiomed.2024.10.280.
48. Holmgren M, Sheets L. Using the Zebrafish lateral line to understand the roles of mitochondria in sensorineural hearing loss. Front Cell Dev Biol. 2021;8: 628712. https://doi.org/10.3389/fcell.2020.628712.
49. Liang S, Dong S, Liu W, Wang M, Tian S, Ai Y, Wang H. Accumulated ROS Activates HIF-1α-induced glycolysis and exerts a protective effect on sensory hair cells against noise-induced damage. Front Mol Biosci. 2022;8: 806650. https://doi.org/10.3389/fmolb.2021.806650.
50. Xiong H, Lai L, Ye Y, Zheng Y. Glucose protects cochlear hair cells against oxidative stress and attenuates noise-induced hearing loss in mice. Neurosci Bull. 2021;37:657–68. https://doi.org/10.1007/s12264-020-00624-1.
51. Burch JS, Marcero JR, Maschek JA, Cox JE, Jackson LK, Medlock AE, Phillips JD, Dailey HA Jr. Glutamine via α-ketoglutarate dehydrogenase provides succinyl-CoA for heme synthesis during erythropoiesis. Blood. 2018;132:987–98. https://doi.org/10.1182/blood-2018-01-829036.
52. Koronowski KB, Khoury N, Saul I, Loris ZB, Cohan CH, Stradecki-Cohan HM, Dave KR, Young JI, Perez-Pinzon MA. Neuronal SIRT1 (Silent Information Regulator 2 Homologue 1) regulates glycolysis and mediates resveratrol-induced ischemic tolerance. Stroke. 2017;48:3117–25. https://doi.org/10.1161/STROKEAHA.117.018562.
53. Beaulac HJ, Gilels F, Zhang J, Jeoung S, White PM. Primed to die: an investigation of the genetic mechanisms underlying noise-induced hearing loss and cochlear damage in homozygous Foxo3-knockout mice. Cell Death Dis. 2021;12:682. https://doi.org/10.1038/s41419-021-03972-6.
54. Yu Q, Du F, Swerdlow RH, Yu H, Chen JX, Yan SS. Antioxidants rescue mitochondrial transport in differentiated alzheimer's disease trans-mitochondrial cybrid cells. Journal of Alzheimer's Disease. 2016;54:679–90. https://doi.org/10.3233/jad-160532.
55. Du H, Guo L, Yan SS. Synaptic mitochondrial Pathology in Alzheimer's disease. Antioxid Redox Signal. 2012;16:1467–75. https://doi.org/10.1089/ars.2011.4277.

56. V. Rangaraju, N. Calloway, T.A. Ryan, Activity-Driven Local ATP Synthesis Is Required for Synaptic Function, Cell 156 (2014). https://doi.org/10.1016/j.cell.2013.12.042.
57. Packer M. Critical reanalysis of the mechanisms underlying the cardiorenal benefits of SGLT2 inhibitors and reaffirmation of the nutrient deprivation signaling/autophagy hypothesis. Circulation. 2022;146:1383. https://doi.org/10.1161/CIRCULATIONAHA.122.061732.
58. Wang D, Yin Y, Wang S, Zhao T, Gong F, Zhao Y, Wang B, Huang Y, Cheng Z, Zhu G, Wang Z, Wang Y, Ren J, Liang G, Li X, Huang Z. FGF1ΔHBS prevents diabetic cardiomyopathy by maintaining mitochondrial homeostasis and reducing oxidative stress via AMPK/Nur77 suppression. Signal Transduct Target Ther. 2021;6:133. https://doi.org/10.1038/s41392-021-00542-2.
59. Wang H, Lin C, Yao J, Shi H, Zhang C, Wei Q, Lu Y, Chen Z, Xing G, Cao X. Deletion of OSBPL2 in auditory cells increases cholesterol biosynthesis and drives reactive oxygen species production by inhibiting AMPK activity. Cell Death Dis. 2019;10:627. https://doi.org/10.1038/s41419-019-1858-9.
60. RC Rabinovitch, B Samborska, B Faubert, EH Ma, SP Gravel, S Andrzejewski, TC Raissi, A Pause, J St.-Pierre, RG Jones. AMPK maintains cellular metabolic homeostasis through regulation of mitochondrial reactive oxygen species. Cell Rep. 21 (2017) 1–9. https://doi.org/10.1016/j.celrep.2017.09.026.
61. Wu F, Hill K, Fang Q, He Z, Zheng H, Wang X, Xiong H, Sha S-H. Traumatic-noise-induced hair cell death and hearing loss is mediated by activation of CaMKKβ. Cell Mol Life Sci. 2022;79:249. https://doi.org/10.1007/s00018-022-04268-4.
62. Zhao R, Ma C, Wang M, Li X, Liu W, Shi L, Yu N. Killer or helper? The mechanism underlying the role of adenylate activated kinase in sound conditioning. Front Synaptic Neurosci. 2022;14:940788. https://doi.org/10.3389/fnsyn.2022.940788.
63. Zhang D, Hu X, Li J, Liu J, Baks-te Bulte L, Wiersma M, Malik NU, van Marion DM, Tolouee M, Hoogstra-Berends F, Lanters EA, van Roon AM, de Vries AAF, Pijnappels DA, de Groot NMS, Henning RH, Brundel BJJM. DNA damage-induced PARP1 activation confers cardiomyocyte dysfunction through NAD+ depletion in experimental atrial fibrillation. Nat Commun. 2019;10(1):1307. https://doi.org/10.1038/s41467-019-09014-2.
64. Ma S, Zhao X, Zhang C, Sun P, Li Y, Lin X, Sun T, Fu Z. Ozone exposure induces metabolic disorders and nad+ depletion through parp1 activation in spinal cord neurons. Frontiers in Medicine. 2020;7: 617321. https://doi.org/10.3389/fmed.2020.617321.
65. Tinkov AA, Nguyen TT, Santamaria A, Bowman AB, Buha Djordjevic A, Paoliello MMB, Skalny AV, Aschner M. Sirtuins as molecular targets, mediators, and protective agents in metal-induced toxicity. Arch Toxicol. 2021;95:2263–78. https://doi.org/10.1007/s00204-021-03048-6.
66. Lan F, Cacicedo JM, Ruderman N, Ido Y. SIRT1 modulation of the acetylation status, cytosolic localization, and activity of LKB1. J Biol Chem. 2008;283:27628–35. https://doi.org/10.1074/jbc.M805711200.
67. Huang Y, Lu J, Zhan L, Wang M, Shi R, Yuan X, Gao X, Liu X, Zang J, Liu W, Yao X. Resveratrol-induced Sirt1 phosphorylation by LKB1 mediates mitochondrial metabolism. J Biol Chem. 2021;297: 100929. https://doi.org/10.1016/j.jbc.2021.100929.

Publisher's Note